



UiT The Arctic University of Norway

Faculty of Engineering Science and Technology

**Analytical Approach to Describe Properties in Transition Zones
Between Ballasted and Non-Ballasted Track**

Analytical Solution to a Beam Resting on a Spring and Damped Foundation with a Moving Load

Joachim Jørgensen Ågotnes

Master's thesis in Engineering Design END-3900 May 2022

ANALYTICAL APPROACH TO DESCRIBE PROPERTIES IN TRANSITION ZONES BETWEEN BALLAST-FREE TRACK AND BALLAST TRACK

FACULTY OF ENGINEERING SCIENCE AND TECHNOLOGY

by

Joachim Jørgensen Ågotnes
B.Sc., Norwegian University of Science and Technology, 2019

Master's Thesis in Engineering Design
END-3900
May 2022



UiT The Arctic
University of Norway

Acknowledgement

This thesis would not have been written if it weren't for Bane NOR. Because of them, a problem description about an interesting topic was published. Throughout this thesis there have been many meetings with Bane NOR where they have shared relevant information and data, and guided the thesis in the right direction.

I would like to thank the two contact persons at Bane NOR:

Dr. Alf Helge Løhren and Celine Chapelier.

During this thesis, stagnation and plateau often hit. Difficult mathematical problems and equations arose with concepts which had to be understood by reading tough theoretical papers on subjects that is hard to comprehend fully. Without the help and support of the team behind me, this thesis wouldn't have been finished in time.

I'd like to express my deepest appreciation to my supervisors:

Professor Anette Meidell and Professor Dag Lukassen.

And also *Dr. Guy Beeri Mauseth, Dr. Andreas Seger and Professor Per Johan Nicklasson*

Lastly, I'd like to thank my fiancée, *Tanita Svenning*, for keeping me motivated and believing in me throughout this process.

Thank you.

Abstract

Norway has for a long time used railways as a means of transport. This method of transportation been used to haul raw materials such as wood and ore. Trains have today become competitors to cars and other means of transportation as a way to commute. However, the tracks used when hauling heavy loads are still being used regardless if the train's goods are commuters or raw materials. Heavy freight trains have a relatively low velocity compared with high-speed trains and because of this, ballasted tracks often used in Norway. The increase in commercial use of train transport has lead to a train-velocity increase and as a result of that, development of non-ballasted tracks have therefore become more favorable. The non-ballasted tracks have a higher stiffness than the ballasted, consequently problems arises when the softer ballasted track transitions over to the stiffer non-ballasted track. Because of the difference in stiffness, will there be a point in the track where the stiffness abruptly changes from one stiffness to another. This will cause damages to the rail, track and train if not dealt with carefully.

The railway company Bane NOR have therefore published an interest in the topic of equalizing the stiffness in transition zones. Gaining a deeper understanding of what happens during a transition zone is important so that unnecessary track degradation can be prevented. However, because of the scarcity of information about this particular topic, this thesis could be beneficial to the community. Transition zones are usually designed based upon prior experiences, and the construction of the zones are commonly done by subcontractors. Bane NOR is therefore aspiring to acquire theoretical models that can describe the rail behaviour in transition zones.

This master's thesis covers the development of an analytical mathematical model that describes the rail's deflection in both ballasted and non-ballasted tracks. The model takes root in an older theory called "*beams on elastic foundation*" [1] and the "*moving force on a beam*" problem. Beams on elastic foundation theory is often used in the railway industry to describe the deflection of rails. Furthermore, the numerical analysis software ANSYS, was utilized to generate an animation of the deflection of the rail beam.

Contents

Acknowledgement	i
Abstract	iii
List of Figures	viii
List of Tables	ix
1 Introduction	1
1.1 Background	1
1.2 Problem Description	3
1.3 The Aim of This Thesis	4
1.4 Problem Limitations	4
1.5 Problem Derivatives	5
1.6 Literature Review	6
2 Design Requirements	9
2.1 Ballasted Track	10
2.2 Non-Ballasted Track	11
3 Analytical Mathematical Modeling	13
3.1 Beam on Elastic Foundation With Moving Load	13
3.2 Equation of Motion	14
3.3 Method	16
4 Numerical Analysis	21
4.1 Elasticity Theory	21
4.2 Design	23
4.3 Transient Structural	24
5 Results and Discussion	29
5.1 Analytical Results	29
5.2 Numerical Results	33
5.3 Discussion	35
6 Further Work and Ideas	37
6.1 Lagrange's Equations	37
6.2 Fourier Transform Method	38
6.3 Deriving the Euler — Lagrange Equation Using Calculus of Variation	39
6.4 Equalization of Elasticity	41

7 Conclusion	43
Appendix	
A Tables	47
B Rail Profile	49
C Vipa DFC	50
D Material Index	55
E Fourier Transform	56
F Master’s Thesis Topic	57
G Material — Sorbothane	63
H MATLAB Code	66
I Other Simulations	68
I.1 7 Meter Beam With 3 Point Distributed Load	68
I.2 1 Meter Beam With Point Load	70
I.3 1 Meter Beam with 3 Point Distributed Load	71
I.4 35 Meter Beam With Point Load	73

List of Figures

1.1	Track components for a general ballasted track [2]	1
1.2	Track components for a general ballastless track, [2]	2
1.3	Illustration of a transition zone [3].	2
1.4	3D illustration of the new train service between Oslo and Ski at the entrance to Oslo S. [4].	3
1.5	The figure illustrates a moving load on a beam [5]	5
1.6	Two illustrations of varying degree of freedom modeled using elastic foundation [1].	5
3.1	Illustration of how a general ballasted track can be modeled. Track components are simplified into a system of mass-spring-dampers.	13
3.2	Simplification from a multi to a single degree-of-freedom system of a railway track.	14
3.3	Infinitesimal section of the beam rail with the forces applied.	14
4.1	Rail profile designed in ANSYS - SpaceClaim	23
4.2	Illustration of the extruded rail profile. The length is 7 m shown in isometric view.	23
4.3	The figure depicts the ANSYS Workbench window where (marked in yellow) Transient Structural toolbox is selected as the project objective.	24
4.4	Engineering Data: Mechanical properties for the material <i>Structural Steel</i>	25
4.5	Meshing data and meshed model	25
4.6	List of time segments.	26
4.7	Springs and dampers connected underneath the rail beam.	27
4.8	Details for the stiffness of the foundation.	27
4.9	Force load vs time graph.	28
4.10	Displacement restriction fixture at each element.	28
5.1	The graph depicts a wave which is the deflection of the rail as the train is moving along the track.	29
5.2	Deflection graph for the ballastless track.	30
5.3	The graph illustrates how the bending moment in the rail behaves when the train moves along the rail in the ballasted section.	31
5.4	Bending moment graph for the ballastless track	31
5.5	Bending stress in both compression and tension of the ballasted side of the track.	32
5.6	Bending stress σ_b for ballastless track	33
5.7	Total deformation of the rail beam at the transition point.	33
5.8	Maximum bending moment in the rail beam	34
5.9	Names to all viable materials	35
5.10	Materials viable for use. Red line is the material index line, green line is the density times Young's modulus line and the blue is the yield stress line.	36
6.1	Ballasted railway track where there are 2 DoF's.	37

B.1	Rail profile of 60E1, [6].	49
D.1	Maximum stored elastic energy in springs [7]	55
H.1	Defining all constants needed to perform the computational analysis.	66
H.2	Solving the equation computationally using MATLAB.	67
H.3	Generating the graphs	67
I.1	The force over time graph.	68
I.2	Force distributed over 3 nodes graph.	68
I.3	The maximum deformation of the distributed load	69
I.4	Maximum bending moment	69
I.5	Deformation of the beam	70
I.6	Force distribution over time	70
I.7	Deformation of the beam when 3 point load was applied	71
I.8	Force distribution over time when 3 point loads were applied	71
I.9	The graph depicts how the 3 point load at a time step looks like	71
I.10	The figure illustrates how the distributed 9 load load were applied at a time step.	72
I.11	The graph is showing how the distributed load looked like vs. time.	72
I.12	Mesh details showing element size to be 500 mm and elements to be 70.	73
I.13	Total force vs. time for 35 meter long beam.	73
I.14	Maximum deformation is showing to be	73
I.15	Total deformation for the beam	74

List of Tables

2.1	Common parameters and values for both ballasted track and non-ballasted track	9
2.2	Coefficients for spring and dampers on the ballasted side and the characteristic length of the ballasted track.	10
2.3	Coefficients for spring stiffness for non-ballasted side and the characteristic length of the ballastless track.	11
5.1	Results from both analytical and numerical analysis	34
5.2	List of materials	36
A.1	Permitted velocity and maximum axle load for superstructure classes, [8].	47
A.2	Rail profile with associated maximum sleeper distance for superstructure classes, [8].	48

Chapter 1

Introduction

1.1 Background

In this paper, the main focus is on an analytical solution for the vertical deflection of a rail beam when a load is applied with constant velocity. An analytical solution for the rail deflection can be utilized in railway design as the deflection of the rails is of great importance.

Railway tracks can broadly be compartmentalized into two groups; *ballast tracks* and *ballastless tracks*. Ballast tracks contains a load bearing material, often referred to as *ballast*. The ballast layer are usually constructed by an assortment of different varieties of crushed rocks which lies on the foundation of the track. A general assembly of ballast track can be seen in Figure 1.1. The ballast plays an important role in track design, as its most important roles are to; support and distribute loads from the train, reducing vibrations inflicted by the train, stabilizing the sleepers, functioning as a drainage system when flooding and a method to keep vegetation at bay [9]. However, in some areas the ballast is undesirable; for instance when driving over a bridge, approaching a road crossing, or in tunnels where the height requirements may prevent the use of ballast.

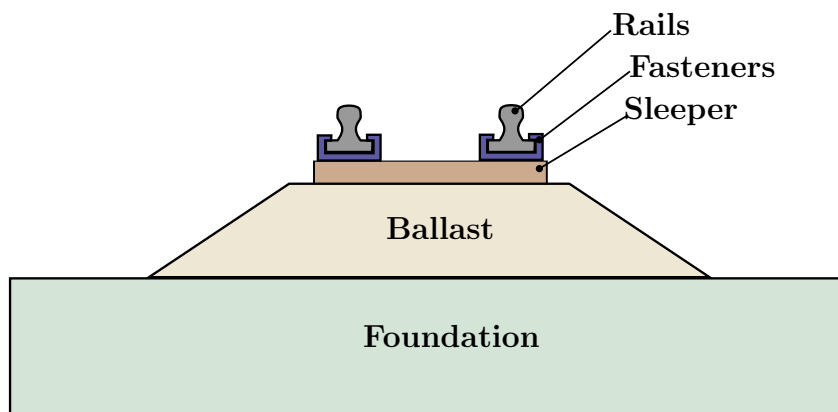


Figure 1.1: Track components for a general ballasted track [2]

Ballastless tracks on the other hand, does not include this layer and will therefore also lack its benefits. Instead, they are constructed using concrete or asphalt, which in result makes the track much stiffer compared to the ballasted ones. Figure 1.2 depicts a general ballastless track schematic. On account of its higher stiffness, the design standardization and production procedure are even more rigorous and as a result the ballastless track is therefore more expensive to construct. Nevertheless, there are advantages to construct tracks without ballast; greater

lifespan, less maintenance, evenly distributing both horizontal and vertical loads, more lenient height requirement compared to conventional ballasted tracks [9].

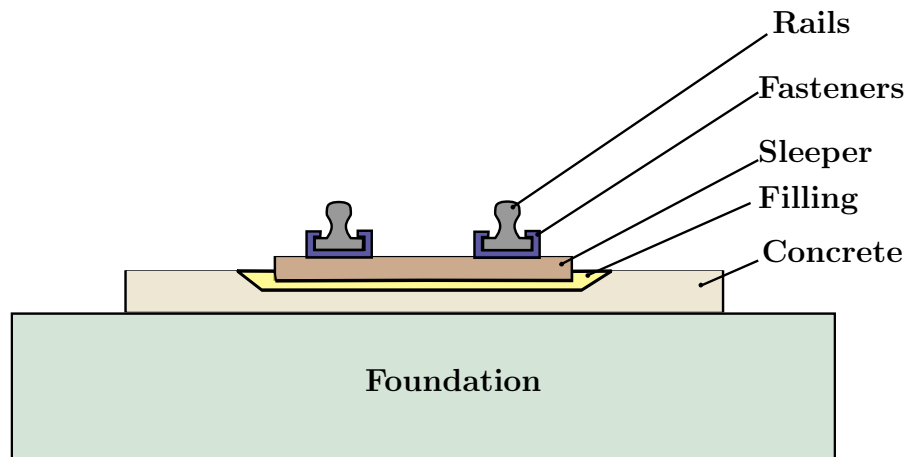


Figure 1.2: Track components for a general ballastless track, [2]

In areas where the track changes from a ballasted track to a non-ballasted track is called a *transition zone* [10]. In these zones the stiffness in the track will abruptly change if the zone's elastic behaviour isn't handled with care. High velocity and heavy train loading can lead to hard rail impact. The rail impact will accelerate the degradation of the rails or worse, can lead to derailment and cause further damages. It is important for both safety, time and resource expenditures to understand what's happening in transition zones and how to avoid these abrupt changes in stiffness. Figure 1.3 illustrates how a transition zone might look like.

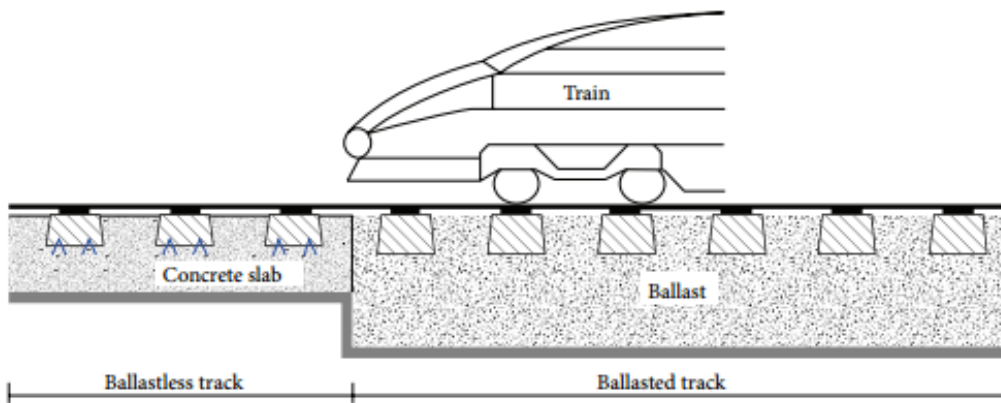


Figure 1.3: Illustration of a transition zone [3].

1.2 Problem Description

An on-going project which is contracted to Bane NOR, is the "Follo line" project [11]. This project aims to shorten the travel time from 22 minutes to 11 minutes from Oslo Central Station (Oslo S.) to Ski station, see figure 1.4 for a 3-dimensional (3D) overview model of the track layout. To achieve this, a tunnel is being constructed. In the tunnel, ballastless track is the optimal choice because of height constraints. Maintenance inside a tunnel can be unsafe and requires both time and resources. However, outside of the tunnel ballast tracks are being utilized and this creates a transition zone issue. As described previously, the transition zone causes a differential settlement due to the difference in elasticity between the two tracks. Furthermore, the Follo Line will experience heavy traffic of high-speed passenger trains and the rails are therefore at a higher risk of degradation. Since this line will be carrying passengers, it's imperative the the transition zone is carefully dealt with, with the best possible solution.



Figure 1.4: 3D illustration of the new train service between Oslo and Ski at the entrance to Oslo S. [4].

The problem formulation were originally developed by Bane NOR and refined and described in cooperation between UiT and Bane NOR. The problem description and master's thesis topic can be found in the Appendix F.

"Railway systems can be of ballast type or non-ballast type. The main railway system in Norway has been of the ballast type. Non-ballast structures are used in areas where for instance ballast is not wanted for instance in bridges, in tunnels with limited heights and possibilities to perform maintenance. Also, high-speed railways are often made of non-ballasted tracks. The combination of ballasted and non-ballasted tracks in different parts of the railway will cause some challenges that must be solved. For instance, in the transition area, the different flexural stiffness of the two types of track design is of great importance. In order to make the transition as smooth as possible the mechanical properties of that part of the railroad must be designed in a best possible

way. The mathematical models that describe this transition area is of great interest to explore and develop in order to be able to design a best possible transition system. In this way, the wear of the track and trains can be as low as possible, at a minimum need for maintenance. The elasticity and dynamical properties of the transition area are of special interest and will be influenced on e.g. type of rails, sleepers, slabs and ballast system. The overall (static and dynamic) behavior of the track system must be according to the requirements of Bane Nor in Norway. The problem formulation is originally developed by Bane Nor and refined and described in cooperation between UiT and Bane Nor.”

1.3 The Aim of This Thesis

The aim of this thesis is to acquire a deeper understanding of railway tracks and getting a perception of the mathematical elasticity problems that faces transition zones and railway tracks today. Using acquired knowledge from researching prior papers on the topic to develop an analytical mathematical model for rail deflection will be the main objective.

A secondary objective is to implement the analytical mathematical model in a numerical analysis software to generate a 3D animation of the rail deflection. Finally, using a material selection software; Granta EduPack to gather materials that can be used to equalize the elasticity in a transition zone.

1.4 Problem Limitations

- The problem will be reduced to a 2 dimensional (2D) problem. The rail is only allowed to deflect in the z -direction.
- The force from the train onto the rail beam will be assumed to be a constant point load moving at a constant speed.
- Only one wheel and rail beam will be considered.
- Assuming constant room temperature; no buckling due to heat nor brittle fracture analysis due to low temperatures.
- Soil foundation is considered to be infinitely stiff and will therefore not be taken into account.
- The springs are assumed to be linear and the dampers are assumed to be viscous [12].
- Assuming the system is a under-damped system.

1.5 Problem Derivatives

The thesis problem can be thought of as a combination of two problems. One of which is the "moving load on a beam" problem and the other "beam on elastic foundation".

Moving Load on a Beam

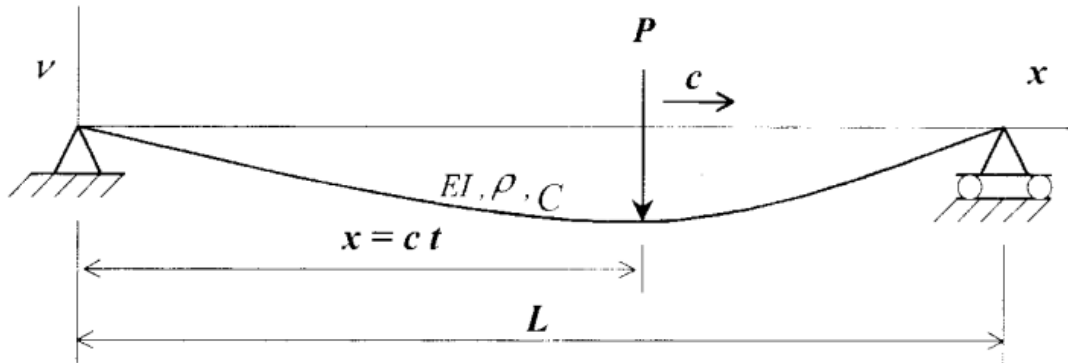
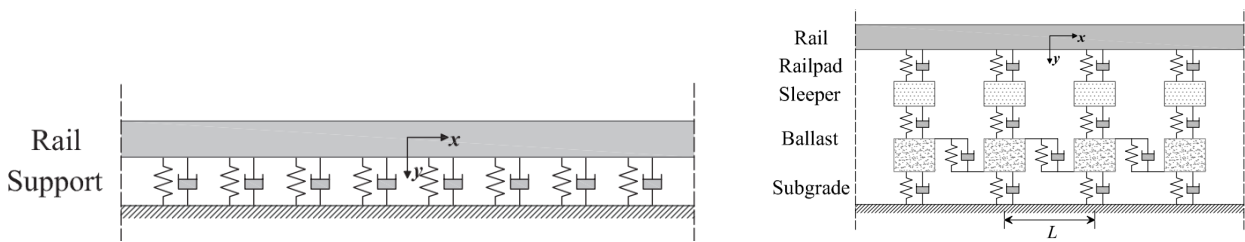


Figure 1.5: The figure illustrates a moving load on a beam [5]

A solution method to this problem were to apply *fast Fourier transform* (FFT) [13], which is a computational method to solve partial differential equation that don't have exact solutions.

Beam on Elastic Foundation

The idea with this theory is that a foundation can be modeled as a system of elastic springs and dampers. If then an infinite beam lies on a foundation the deflection of the beam can be measured based on the contraction of the springs and dampers. Furthermore the foundation model can have multiple degrees of freedom. The figure 1.6 illustrates a single degree of freedom system 1.6a, and multiple degrees of freedom system 1.6b.



(a) Elastic foundation model of single degree of freedom system

(b) Elastic foundation model of multiple degrees of freedom system

Figure 1.6: Two illustrations of varying degree of freedom modeled using elastic foundation [1].

1.6 Literature Review

Railway systems are very intricate with many moving parts and parameters that can be near impossible to accurately describe mathematically. Because of the complexity, engineers and scientists use approximations and simplifications when the physics are too problematical to model. The necessity for simplifications leads to models that does not accurately describe the real-life scenario. However, as more attention is brought on this topic and that science is advancing, the models are progressively becoming more accurate.

Issues Related to Transition Zones — Problem

The report [14], convey issues and the complexity of the structural dynamic problems in railway transition zones. The author writes that track degradation's main problem is; the differential settlement and the enhanced dynamical loads which causes an abrupt change in stiffness. Sudden stiffness divergences can only be regulated if the transition zones could be smoothed out, resulting in a gradual transition zone. The author also states that most of the currently available designs are influenced through trail and error — moreover, model parameters are unreliable as they are regulated to local subgrade and ballast. The author is expressing problems when facing transition zones, and conveys that even attempting to fix the issue or if FEM analysis were relevant; the design and model will not correlate. The models are too imprecise for estimations and unveil noticeable deviation when compared to field data.

Beams on Elastic Foundation — Solution

The research paper [1], conducts an extensive state-of-the-art technical review of *beams on elastic foundation* — or, BOEF for short. BOEF is a vastly applicable theory and even so, in studying the behaviour of railway tracks. The theory can used to simulate the periodic nature of railways, as well as the different layers that the railway track consists of. The theory is originated from mass-spring-damper systems, thus the complexity in the modeling, and the simulation run time can drastically be lowered, yet maintaining accuracy. The team behind this research paper have conducted an extensive review of many methods that are applicable to railways. This paper contains many mathematical models that describes various phenomena that occurs on the railway tack. The models are graded on a star system (1-5) on how accurate and applicable they are.

Optimization by Applying Under-Sleeper-Pads — Solution

A transition zone in a tunnel; Turecky Vrch [15], has lead to some problems when transitioning between railway types where the bending stiffness's deviate. By implementing ANSYS for modeling it was found that a mathematical model can be established. The model found that by utilizing stiffening rails and under sleeper pads; the vertical deflection, speed and acceleration could be measured. However, comparing the results, the stiffening rails were deemed to be an insignificant improvement. Nevertheless, application of the under sleeper pads optimized the transition area when; the placement, shape and thickness of the pads were settled.

Decreasing Stiffness in Rubber Mats — Solution

The report [16], written by a group who's researching transition zones between different types of slab track. Due to differential settlement as well as the abrupt change in track stiffness, major vibrations and track deterioration occurs. To confirm the necessity to gradually change the stiffness in transition zones, the dynamic responses to a self compiling vehicle-track program

were analyzed. To achieve a smoother transition zone, the use of rubber mats were proposed. Five rubber mats which varied in stiffness ranging from 160 MN/m^3 down to 20 MN/m^3 , were placed down on the track to gradually increase/ decrease the stiffness. The results showed that; instead of an abrupt violent impact, it is dispersed over a longer distance. However, the stiffness in each rubber mat in the transition zone must be determined by case.

Baseplate Fastening System — Solution

[17] Solution to the stiffness transition zone problems by implementing an application of baseplate fastening system. The research team utilized numerical models through the software LS-DYNA, and furthermore validating the simulation by comparing with field measurements. The team gathered that soft baseplate pads intensified the deflection of the rail. Moreover, the weight of the baseplate had a slight role in reducing the differential settlement. However, the team also obtained that a pad stiffness of 400 MN/m^3 resulted in the best solution as the slab track stiffness can be equalised to the stiffness of ballasted track. On the other hand, softer and heavier baseplate pads together may cause negative effect by increasing the rail deflection and therefore a higher differential settlement. Overall, carefully selecting the optimum baseplate specification to the stiffness in the transition zone the problem can be solved.

Requirements for Transitions — Solution

In the book, Modern Railway track [18], it is stated that when it comes to transition zones, it is required that sleepers have to be anchored to the substructure at a distance of minimum 10 meters. Further, the author writes that when transitioning from slab track to ballast track, the railways behaves differently regarding stiffness, flexibility and settlement behavior. To make them more compatible with one another can be achieved in several ways:

Stiffness Incrementally decreasing the fastening's elasticity.

Flexibility Implementation of additional rails for 20 meters.

Settlement Using chemical binders to increase the ballast's resistance to shear.

Settlement and Flexibility Extending the concrete roadbed with an increasing taper for at least 10 meters to stiffen the ballasted track.

Chapter 2

Design Requirements

Some general parameters are defined by Bane NOR is listed in Table 2.1. The Follo Line is being designed for train velocities at 250 km/h and axle load of 18 tons, it has been determined that more conservative calculation are of interest in this study and the axle load is therefore increased to 22.5 tons, although only *one* wheel will be taking into consideration. Geometrical properties of the rail profile, rail mass and sleeper distance were defined from tables in the Appendix A and the mechanical drawing of the rail profile in Appendix B.

Since the track contains a transition zone from ballasted track to non-ballasted, the tracks have unique parameters associated that will describe them. However, some parameters are consistent for both tracks regardless of substructure and other elements. The length of a transition zone, L_x is defined in the technical standard *NS-EN 16432-2* to be half of the velocity classification of the track [19].

Symbol	Value	Unit	Explanation
E	210×10^9	Pa	Young's modulus rail
Q	11×10^6	N	Train's load per wheel
v	70.0	m/s	Train's velocity
I	3.0383×10^{-5}	m^4	Second moment of area
d_s	0.6	m	Distance between each sleeper
A	76.7×10^{-4}	m	Cross sectional area of rail
μ	60.34	kg/m	Density of rail beam
L_x	35.0	m	Length of transition zone

Table 2.1: Common parameters and values for both ballasted track and non-ballasted track

2.1 Ballasted Track

The ballast will have a continuous spring stiffness and damping, the spring stiffness and damping from the padding on the other hand, are discrete values that lie on top of each sleeper. To determine a continuous contribution from the padding, the spring and damping coefficients for the pads in Table 2.2 are dispersed values over the distance between each sleeper, d_s . Approximation of a continuous support can be calculated using this formula [18]

$$k \approx \frac{k_d}{d_s} \quad (2.1)$$

Where k_d is the discrete spring stiffness of the padding support. In this analysis the padding stiffness is $k_d = 50 \times 10^6$ N/m.

Symbol	Value	Unit	Explanation
k_b	65×10^6	N/m^2	Spring coefficient of ballast
c_b	150×10^3	Ns/m^2	Damping coefficient of ballast
k_p	83.33×10^6	N/m^2	Spring coefficient of the padding
c_p	8.33×10^3	Ns/m^2	Damping coefficient for padding
L_c	0.9	m	Characteristic length

Table 2.2: Coefficients for spring and dampers on the ballasted side and the characteristic length of the ballasted track.

In the ballasted section of the track there are two kinds of stiffness and damping which occur; ballast and padding. These coefficients lie in series and can be added together to form an equivalent spring and damper. Using the relation that when two springs and dampers are in series they can be added in the following way, [12]:

$$k_{eq} = \frac{k_b k_p}{k_b + k_p} = 3.65 \times 10^7 \quad (2.2)$$

$$c_{eq} = \frac{c_b c_p}{c_b + c_p} = 7.89 \times 10^3 \quad (2.3)$$

Another parameter is the characteristic length of the track [18] which is given by

$$L_c = \sqrt[4]{\frac{4EI d_s}{k_d}} = \sqrt[4]{\frac{4EI}{k_{eq}}} \quad (2.4)$$

The characteristic length for the ballasted section can be calculated to be $L_c = 0.9$ meters

2.2 Non-Ballasted Track

The fastening system being utilized at the ballastless side is the *Vipa DFC* model, see Appendix C for the product specification. The fastening system is used in Rheda 2000 tracks [20]. The fastening system contains padding to increase the flexibility as the foundation is made of solid concrete which is considered to be infinitely stiff. The pads are designed with a dynamical stiffness of $k_d = 20 - 30$ kN/mm although, since the pads lie on top of the sleepers they are discrete values. Nevertheless, as in the ballasted section the padding stiffness can be dispersed over the sleeper distance d_s to make it continuous. The characteristic length of the ballastless track can be calculated to be $L_c = 0.88$ meters. According to information conveyed by Bane Nor, there is little to no damping in the non-ballasted track. Using the average equivalent dynamic stiffness from the Vipa DFC, the coefficient for spring stiffness is:

Symbol	Value	Unit	Explanation
k_{eq}	4.17×10^7	N/m^2	Spring coefficient for non-ballasted track
L_c	0.88	m	Characteristic length

Table 2.3: Coefficients for spring stiffness for non-ballasted side and the characteristic length of the ballastless track.

Chapter 3

Analytical Mathematical Modeling

3.1 Beam on Elastic Foundation With Moving Load

Literature on the topic of track modeling often references *beams on elastic foundations* (BOEF). An in-dept report specifically wrote a review about the versatile use this method is for railway modeling, [1]. The method is based upon a dynamical systems approach such as; mass-spring-damper with multi degree-of-freedom. Figure 3.1 illustrates how a rail and sleepers resting on ballast can be modelled using BOEF theory.

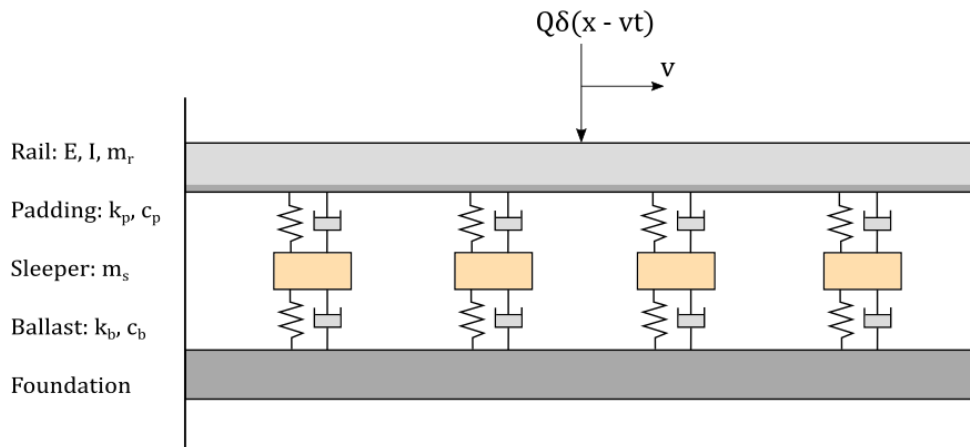


Figure 3.1: Illustration of how a general ballasted track can be modeled. Track components are simplified into a system of mass-spring-dampers.

Figure 3.1 depicts a model that is referred to as a "*Two-layered Winkler foundation*" [1], where a continuous Euler-Bernoulli beam rests on discrete sleepers; and by extension the padding and the ballast. The placement of the sleepers adds to the complexity, as additional reaction forces arise whenever the moving load transverse's each sleeper. The Two-layered model will also add to the degree of freedom (DoF), which are two in this case. Dynamical systems that involves multiple DoFs; with a moving load can become near impossible to solve analytically and computational approximations are usually required to generate a solution. However, utilizing the core concepts of BOEF theory, a simplification of this model can be used, see Figure 3.2.

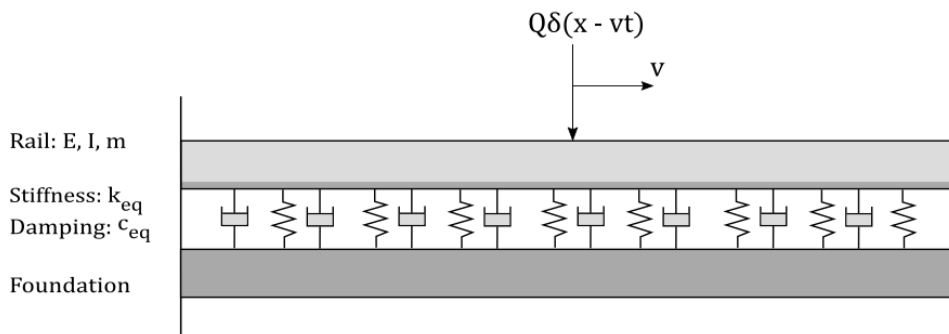


Figure 3.2: Simplification from a multi to a single degree-of-freedom system of a railway track.

A simplification can reduce the model to a single DoF system which can be analytically solved, though it will lessen the control of the parameters and accuracy of the model. Removing the mass of the sleepers altogether, the stiffness and damping coefficients can be merged into equivalent stiffness and damping coefficients.

This simplified model is referred to as a "Single-layered Winkler foundation" and can be used to model both ballasted tracks and non-ballasted tracks by varying the spring and damper coefficients appropriately, the terms k_b and c_b are negated for the ballastless side. Using this simpler model it becomes clear that the control and accuracy of the stiffness parameters lowers.

3.2 Equation of Motion

To derive the governing equation of the model, an infinitesimal section of the rail beam is cut out, see Figure 3.3.

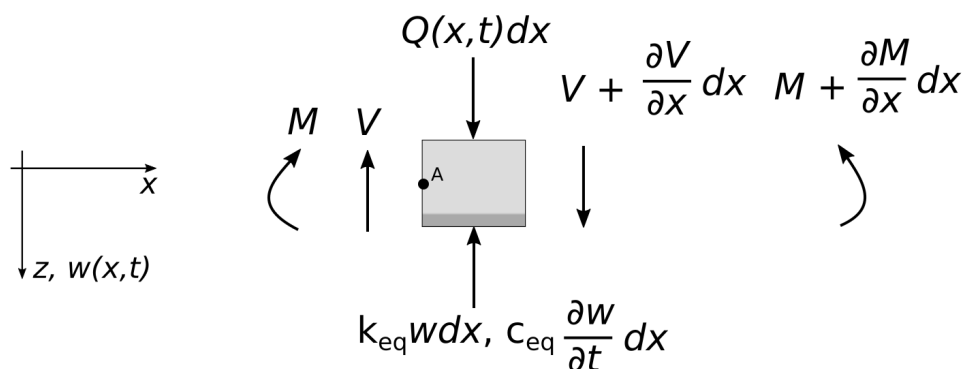


Figure 3.3: Infinitesimal section of the beam rail with the forces applied.

Using Newton's second law,

$$F = ma$$

the sum of all forces in the z direction must equal $m\ddot{w}$ due to the movement of the beam.

$$+\downarrow \sum F_z = \mu A dx \frac{\partial^2 w}{\partial t^2} \quad (3.1)$$

Where, μ is the mass per length and A is the cross sectional area of the beam.

$$\mu A dx \frac{\partial^2 w}{\partial t^2} = -V + V + \frac{\partial V}{\partial x} dx + Q(x, t) dx - k_{eq} w dx - c_{eq} \frac{\partial w}{\partial t} dx \quad (3.2)$$

$$\mu A \frac{\partial^2 w}{\partial t^2} + k_{eq} w + c_{eq} \frac{\partial w}{\partial t} = \frac{\partial V}{\partial x} + Q(x, t) \quad (3.3)$$

Since the beam is an Euler-Bernoulli beam, the moment must equal to zero.

$$\zeta + \sum M_A = 0:$$

$$M + \frac{\partial M}{\partial x} dx - M - (V + \frac{\partial V}{\partial x} dx) dx + \frac{1}{2} k_{eq} w dx^2 + \frac{1}{2} c_{eq} \frac{\partial w}{\partial t} dx^2 + \frac{1}{2} Q(x, t) dx^2 = 0 \quad (3.4)$$

In comparison to dx , will $dx^2 \approx 0$, and Eq. (3.4) becomes:

$$V = \frac{\partial M}{\partial x} \quad (3.5)$$

Inserting Eq. (3.5) into Eq. (3.3) gives:

$$\mu A \frac{\partial^2 w}{\partial t^2} + c_{eq} \frac{\partial w}{\partial t} + k_{eq} w = \frac{\partial^2 M}{\partial x^2} + Q(x, t) \quad (3.6)$$

The moment in an Euler-Bernoulli beam can be expressed as:

$$M(x, t) = -EI \frac{\partial^2 w(x, t)}{\partial x^2} \quad (3.7)$$

Inserting Eq. (3.7) into Eq. (3.6) results in the partial differential equation for the model:

$$EI \frac{\partial^4 w}{\partial x^4} + \mu A \frac{\partial^2 w}{\partial t^2} + c_{eq} \frac{\partial w}{\partial t} + k_{eq} w = Q \delta(x - vt) \quad (3.8)$$

Eq. (3.7) represents an Euler-Bernoulli beam resting on a foundation with constant springs and dampers and a moving load denoted as $Q \delta(t - vt)$, there $\delta(\cdot)$ is the Dirac delta function.

Typically when there are higher ordered differential equations in which damping occur, *three* cases arises.

- i)* Critically damped system
- ii)* Over-damped system
- iii)* Under-damped system

It is assumed that the track is an under-damped system and cases *i)* - *ii)* are therefore neglected in this analysis.

3.3 Method

There are many techniques to solve a partial differential equation (PDE), however it's mainly to simplify the PDE to an easier PDE or to reduce it to an ordinary differential equation (ODE). The equation of motion is a PDE because the deflection $w(x, t)$ depends on both the positioning x and the time t .

One method of solving this is to use a technique called *change of coordinates* [21]. Because of the movement of the train, changing the coordinate system from a stationary one to a coordinate system that follows the train's velocity will simplify the PDE to a ODE. The variables x and t becomes variables to another function $\xi(x, t)$. The deflection will therefore only be in terms of *one* variable.

The new variable can be expressed in terms of x and t as follows:

$$\xi = x - vt \quad (3.9)$$

The new variable have the dimension of $[m]$, and represents the distance relative from the trains load point. The deflection can therefore be written in it's new form:

$$w(x, t) \rightarrow w(\xi) = w(x - vt) \quad (3.10)$$

Using the new coordinate from Eq. (3.10), the derivatives are calculated using the chain rule for multi variable functions.

$$\frac{\partial^4 w(\xi)}{\partial x^4} = \frac{d^4 w(\xi)}{d\xi^4} \quad (3.11)$$

$$\frac{\partial w(\xi)}{\partial t} = -v \frac{dw(\xi)}{d\xi} \quad (3.12)$$

$$\frac{\partial^2 w(\xi)}{\partial t^2} = v^2 \frac{d^2 w(\xi)}{d\xi^2} \quad (3.13)$$

Inserting these into Eq. (3.8) yields:

$$EI \frac{d^4 w(\xi)}{d\xi^4} + v^2 \mu A \frac{d^2 w(\xi)}{d\xi^2} - v c_{eq} \frac{dw(\xi)}{d\xi} + k_{eq} w(\xi) = Q \delta(\xi) \quad (3.14)$$

Because of the change in variables, the steady state solution is not of interest but rather the transient solution is. The wave propagation, which is caused by initial values and boundary conditions, is set stabilize further away from the train's contact point. Therefore, the homogeneous equation can be expressed as:

$$\frac{d^4 w(\xi)}{d\xi^4} + \left(\frac{v^2 \mu A}{EI} \right) \frac{d^2 w(\xi)}{d\xi^2} - \left(\frac{v c_{eq}}{EI} \right) \frac{dw(\xi)}{d\xi} + \left(\frac{k_{eq}}{EI} \right) w(\xi) = 0 \quad (3.15)$$

This expression can be further simplified to:

$$\frac{d^4w(\xi)}{d\xi^4} + 4(\alpha\lambda)^2\frac{d^2w(\xi)}{d\xi^2} - 8\alpha\beta\lambda^3\frac{dw(\xi)}{d\xi} + 4\lambda^4w(\xi) = 0 \quad (3.16)$$

Where $\lambda = \left(\frac{k_{eq}}{4EI}\right)^{1/4}$ is the static wave characteristics. The parameter $\alpha = \frac{v}{v_{cr}}$ is the velocity ratio, where the critical velocity is defines as $v_{cr} = \left(\frac{4k_{eq}EI}{(\mu A)^2}\right)^{1/4}$. The critical velocity is the minimum velocity at which a free wave may propagate in an infinite beam. The damping ratio is defined as the ratio of the actual damping to the critical damping $\beta = \frac{\beta}{\beta_{cr}}$ where the critical damping is $\beta_{cr} = 2\sqrt{k_{eq}\mu A}$.

One general solution to the equation is to guess a solution. A typical method to solve these types of ODE's is to assume the solution takes the form:

$$w(\xi) = e^{\gamma\xi} \quad (3.17)$$

Using the general solution leads to the characteristic equation:

$$\gamma^4 + 4(\alpha\lambda)^2\gamma^2 - 8\alpha\beta\lambda^3\gamma + 4\lambda^4 = 0 \quad (3.18)$$

An n -th degree polynomial will always have n roots whenever n is even. Eq. 3.18 is of degree *four* and will therefore have four roots. Generally; $\gamma_1 = a_1 + ib_1$, $\gamma_2 = a_1 - ib_1$, $\gamma_3 = a_2 + ib_2$ and $\gamma_4 = a_2 - ib_2$. The roots can be factorized:

$$(\gamma - (a_1 + ib_1))(\gamma + (a_1 - ib_1))(\gamma - (a_2 + ib_2))(\gamma + (a_2 - ib_2)) = 0 \quad (3.19)$$

However, when considering a under-damped system, the four roots will have the same real part, meaning; $a_1 = a_2 = a$. The roots can therefore be written as; $\gamma_1 = a + ib_1$, $\gamma_2 = a - ib_2$, $\gamma_3 = -a + ib_1$ and $\gamma_4 = -a - ib_2$. The roots can be expressed as such:

$$(\gamma - a - ib_1)(\gamma - a + ib_2)(\gamma + a - ib_1)(\gamma + a + ib_2) = 0 \quad (3.20)$$

Expanding and simplify Eq. (3.20) it becomes:

$$\gamma^4 + (-2a^2 + b_1^2 + b_2^2)\gamma^2 - 2a(b_2^2 - b_1^2)\gamma + (a^2 + b_1^2)(a^2 + b_2^2) = 0 \quad (3.21)$$

Comparing the coefficients of Eq. (3.18) and Eq. (3.21), it becomes clear that these must be equal:

$$4(\alpha\lambda)^2 = -2a^2 + b_1^2 + b_2^2 \quad (3.22)$$

$$-8\alpha\beta\lambda^3 = -2a(b_2^2 - b_1^2) \quad (3.23)$$

$$4\lambda^4 = (a^2 + b_1^2)(a^2 + b_2^2) \quad (3.24)$$

Using the above equations, it can be shown that b_1^2 and b_2^2 can be expressed in terms of the other variables. From Eq. (3.22), b_2^2 can be expressed as:

$$b_2^2 = 4\alpha^2\lambda^2 + 2a^2 - b_1^2 \quad (3.25)$$

Inserting this into Eq. (3.23) leads to the following:

$$-8\alpha\beta\lambda^2 = -2a(4\alpha^2\lambda^2 + 2a^2 - 2b_1^2) \quad (3.26)$$

$$b_1^2 = a^2 - \frac{2\alpha\beta\lambda^3}{a} + 2\alpha^2\lambda^2 \quad (3.27)$$

Inserting back into the expression for b_2^2 :

$$b_2^2 = a^2 + \frac{2\alpha\beta\lambda^3}{a} + 2\alpha^2\lambda^2 \quad (3.28)$$

Inserting the results for b_1^2 and b_2^2 into Eq. (3.24) and make some simplifications, the coefficients can be expressed in terms of a and Eq. (3.18) can be rewritten as:

$$a^6 + 2(\alpha\lambda)^2a^4 + \lambda^4(\alpha^4 - 1)a^2 - \alpha^2\beta^2\lambda^6 = 0 \quad (3.29)$$

It is assumed that a , is the characteristic length of a free wave [m^{-1}], and can therefore be expressed as two variables $a = \eta\lambda$, where λ is the characteristic length and η is the positive and real root of:

$$\eta^6 + 2\alpha^2\eta^4 + (\alpha^4 - 1)\eta^2 - \alpha^2\beta^2 = 0 \quad (3.30)$$

General solution to a homogeneous differential equation as seen in Eq. (3.16) is given by:

$$w(\xi) = e^{-a\xi}(C_1 \sin b_2\xi + C_2 \cos b_2\xi) + e^{a\xi}(C_3 \sin b_1\xi + C_4 \cos b_1\xi) \quad (3.31)$$

Where, C_1, C_2, C_3 and C_4 are constants of integration. When the load is concentrated at the origin ($\xi = 0$), it's reasonable to assume that the slopes and deflections of the beam are zero as $\xi \rightarrow \pm\infty$. By assuming this, it is required that the deflection must be:

$$w(\xi) = \begin{cases} e^{-a\xi}(C_1 \sin b_2\xi + C_2 \cos b_2\xi) & \text{for } \xi \geq 0 \\ e^{a\xi}(C_3 \sin b_1\xi + C_4 \cos b_1\xi) & \text{for } \xi < 0 \end{cases} \quad (3.32)$$

The beam's boundary condition requires the deflection, slope and bending moment to be continuous across the origin. The shear force on the other hand, has a discontinuity of $\frac{Q}{EI}$ around the origin. The boundary conditions can be expressed as:

$$\lim_{\varepsilon \rightarrow 0} [w(0 + \varepsilon) - w(0 - \varepsilon)] = 0 \quad (3.33)$$

$$\lim_{\varepsilon \rightarrow 0} [w'(0 + \varepsilon) - w'(0 - \varepsilon)] = 0 \quad (3.34)$$

$$\lim_{\varepsilon \rightarrow 0} [w''(0 + \varepsilon) - w''(0 - \varepsilon)] = 0 \quad (3.35)$$

$$\lim_{\varepsilon \rightarrow 0} [w'''(0 + \varepsilon) - w'''(0 - \varepsilon)] = \frac{Q}{EI} \quad (3.36)$$

Taking the appropriate derivatives of $w(\xi)$ and utilizing the boundary conditions, the following relations can be established between the constants of integration C_n for $n = 1, 2, 3, 4$:

$$C_1 = \frac{b_1^2 - b_2^2 + 4\eta^2\lambda^2}{4\eta\lambda b_2} C_2 \quad (3.37)$$

$$C_3 = \frac{b_1^2 - b_2^2 - 4\eta^2\lambda^2}{4\eta\lambda b_1} C_2 \quad (3.38)$$

$$C_2 = C_4 = \frac{4Q\eta\lambda}{EI [4\eta^2\lambda^2(4\eta^2\lambda^2 + b_2^2 + 3b_1^2) + (b_2^2 - b_1^2)(4\eta^2\lambda^2 - b_1^2 + b_2^2)]} \quad (3.39)$$

Letting $a = \eta\lambda$ and substituting in for b_1^2 and b_2^2 , the constants can be expressed as follows:

$$C_1 = \frac{\eta^3 - \alpha\beta}{\lambda\eta(\eta^3 + 2\alpha^2\eta + 2\alpha\beta)} C_2 \quad (3.40)$$

$$C_3 = -\frac{\eta^3 + \alpha\beta}{\lambda\eta(\eta^3 + 2\alpha^2\eta - 2\alpha\beta)} C_2 \quad (3.41)$$

$$C_2 = C_4 = \frac{Q\eta}{4EI\lambda^2(2\eta^6 - 2\alpha^2\lambda\eta^4 + \alpha^2\beta^2\lambda)} \quad (3.42)$$

Furthermore; the deflection $w(\xi)$ can be expressed explicitly as:

For $\xi \geq 0$:

$$w(\xi) = \frac{Q\eta e^{-\lambda\eta\xi}}{4EI\lambda^2(2\eta^6 - 2\alpha^2\lambda\eta^4 + \alpha^2\beta^2\lambda)} \times \left[\frac{\eta^3 - \alpha\beta}{\lambda\eta(\eta^3 + 2\alpha^2\eta + 2\alpha\beta)} \sin \left(\left[\eta^2 + \frac{2\alpha\beta}{\eta} + 2\alpha^2 \right]^{1/2} \lambda\xi \right) + \cos \left(\left[\eta^2 + \frac{2\alpha\beta}{\eta} + 2\alpha^2 \right]^{1/2} \lambda\xi \right) \right] \quad (3.43)$$

For $\xi < 0$:

$$w(\xi) = \frac{Q\eta e^{\lambda\eta\xi}}{4EI\lambda^2(2\eta^6 - 2\alpha^2\lambda\eta^4 + \alpha^2\beta^2\lambda)} \times \left[-\frac{\eta^3 + \alpha\beta}{\lambda\eta(\eta^3 + 2\alpha^2\eta - 2\alpha\beta)} \sin \left(\left[\eta^2 - \frac{2\alpha\beta}{\eta} + 2\alpha^2 \right]^{1/2} \lambda\xi \right) + \cos \left(\left[\eta^2 - \frac{2\alpha\beta}{\eta} + 2\alpha^2 \right]^{1/2} \lambda\xi \right) \right] \quad (3.44)$$

Chapter 4

Numerical Analysis

Numerical analysis is a branch in mathematics to approximate solutions to problems where exact solutions doesn't exist. Numerical analysis is therefore a powerful tool that can provide a solution although not the exact. The approximation is an iterative process and the solutions can have very high accuracy depending on the numerical method that's being used.

4.1 Elasticity Theory

Finite element analysis (FEA) is often used by engineers to analyse a geometry with given boundary and initial conditions. The finite element method subdivides the geometry into smaller elements and solves the mathematical problem for each element. Because of the subdivision of the geometry this method is discrete and can only approximate a solution. In the field of structural mechanics the deflection of a geometry after a given force is important. FEA generates a solution of the deflection based upon a reformulation of Hooke's law [22].

$$\sigma_{ij} = \sum_{k=1}^3 \sum_{l=1}^3 c_{ijkl} \varepsilon_{kl} \quad (4.1)$$

Where σ_{ij} is the stress tensor, ε_{kl} is the strain tensor and c_{ijkl} is a fourth order stiffness tensor and can be thought to be the linear map between the second order tensors.

$$\sigma_{ij} = \begin{bmatrix} \sigma_{11} & \sigma_{12} & \sigma_{13} \\ \sigma_{21} & \sigma_{22} & \sigma_{23} \\ \sigma_{31} & \sigma_{32} & \sigma_{33} \end{bmatrix} \quad (4.2)$$

$$\varepsilon_{kl} = \begin{bmatrix} \varepsilon_{11} & \varepsilon_{12} & \varepsilon_{13} \\ \varepsilon_{21} & \varepsilon_{22} & \varepsilon_{23} \\ \varepsilon_{31} & \varepsilon_{32} & \varepsilon_{33} \end{bmatrix} \quad (4.3)$$

The stiffness tensor c_{ijkl} will contain 81 real numbers, however due to symmetrical properties for the stress and strain tensor the stiffness tensor can be reduced to only containing 21 values and the stress and strain tensor are reduced to only 6. The symmetrical properties of the material can further reduce the stiffness tensor. Materials that have different properties that depend on direction are called *Anisotropic* materials [22]. *Isotropic* materials will have identical properties

in all directions. *Orthotropic* materials will have different properties in mutually perpendicular directions.

Metal is an isotropic material and the stiffness tensor can be reduced to only two numbers; the bulk modulus K and the shear modulus G . The bulk modulus represent the material's response to hydrostatic pressure, while the shear modulus is the material's response to shear stress. These moduli can be written in terms of the Young's modulus, which is the material's strain response to directional stress, and the Poisson's ratio which is the orthogonal strain response to the directional stress [22]. These moduli are related in the following way

$$E = 2G(1 + \nu) = 3K(1 - 2\nu) \quad (4.4)$$

For isotropic materials, Hooke's law Eq. (4.1) can be represented as such:

$$\begin{bmatrix} \sigma_{11} \\ \sigma_{22} \\ \sigma_{33} \\ \tau_{23} \\ \tau_{13} \\ \tau_{12} \end{bmatrix} = \frac{E}{(1 + \nu)(1 - 2\nu)} \begin{bmatrix} 1 - \nu & \nu & \nu & 0 & 0 & 0 \\ \nu & 1 - \nu & \nu & 0 & 0 & 0 \\ \nu & \nu & 1 - \nu & 0 & 0 & 0 \\ 0 & 0 & 0 & \frac{1-2\nu}{2} & 0 & 0 \\ 0 & 0 & 0 & 0 & \frac{1-2\nu}{2} & 0 \\ 0 & 0 & 0 & 0 & 0 & \frac{1-2\nu}{2} \end{bmatrix} \begin{bmatrix} \varepsilon_{11} \\ \varepsilon_{22} \\ \varepsilon_{33} \\ \gamma_{23} \\ \gamma_{13} \\ \gamma_{12} \end{bmatrix} \quad (4.5)$$

FEA uses an equation such as Eq. (4.5) on each element of the subdivided 3D geometry to calculate the stresses in the model.

4.2 Design

A numerical analysis has been done in the computer software ANSYS. The aim was to model the cross-sectional area of the rail beam that is being used by Bane Nor at the Follo line. The rail profile was been designed using the dimensions found in Appendix B.

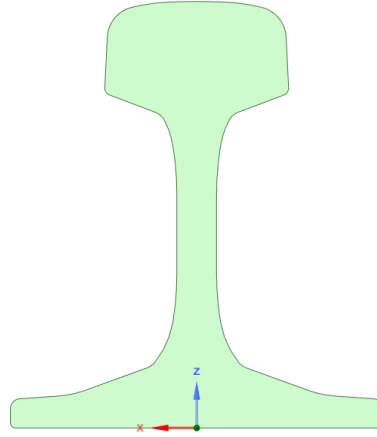


Figure 4.1: Rail profile designed in ANSYS - SpaceClaim

The rail profile were extruded to 7 meters where half of the beam is in the ballasted section and the other in the non-ballasted section. The transition zone L_x is actually 35 meters, however a 7 meter long segment will be sufficient as long as it's no longer than at least five times the characteristic length of the track [18]. Recall that the characteristic length for the non-ballasted section is $L_c = 0.88$ meters which corresponds to a minimum needed length of 4.4 meters, which is more than half the of the section. For the ballasted section the characteristic length was $L_c = 0.9$ meters which corresponds to a minimum length of 4.5 meters which is also more than half of the beam segment being analyzed.

According to Euler - Bernoulli beam theory [23] the slenderness ratio, which is the height to length ratio, should be less than $1/15$. The height is 172 mm and the length is 7000 mm which results in a slenderness ratio of 0.0245. Also, there are many more elements in the longitudinal direction versus the deflection direction.

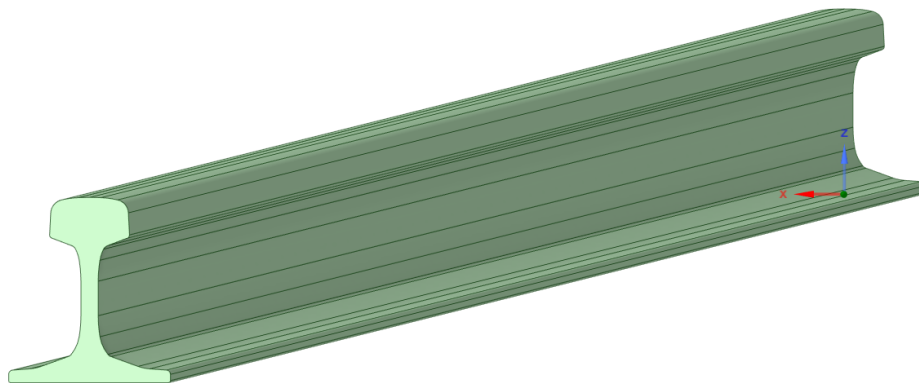


Figure 4.2: Illustration of the extruded rail profile. The length is 7 m shown in isometric view.

4.3 Transient Structural

The interaction of the train's wheel onto the rail causes a moving load on the beam. The position of the load is constantly updating along the beam and is therefore not a *static structural* problem, but rather a *transient structural* problem.

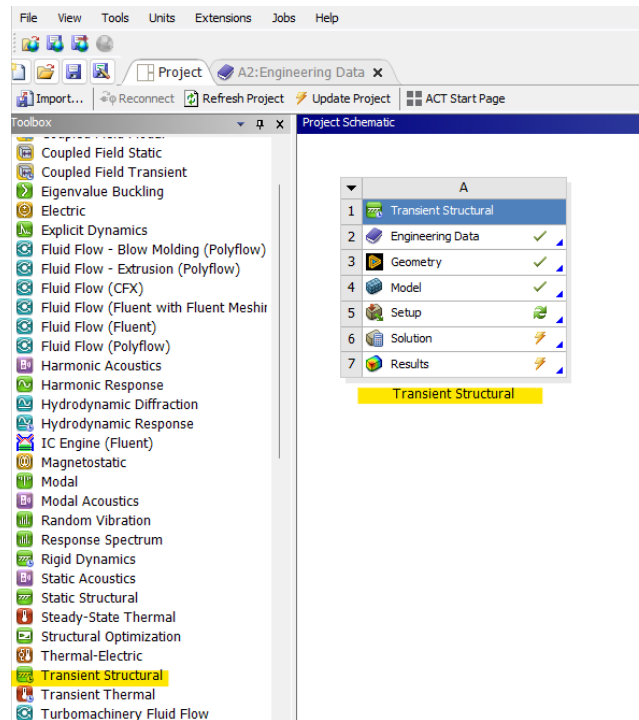


Figure 4.3: The figure depicts the ANSYS Workbench window where (marked in yellow) Transient Structural toolbox is selected as the project objective.

Engineering Data

The material used for the rail beam is structural steel with similar mechanical properties as seen in Table 2.1.

The screenshot shows two windows. The top window, 'Outline of Schematic A2: Engineering Data', lists the material 'Structural Steel' with its source 'General_Materials.xml' and a description of fatigue data. The bottom window, 'Properties of Outline Row 3: Structural Steel', is a table of mechanical properties.

Property	Value	Unit
Material Field Variables	Table	
Density	7850	kg m ⁻³
Isotropic Secant Coefficient of Thermal Expansion		
Isotropic Elasticity		
Derive from	Young's Modulus and Poisson...	
Young's Modulus	2E+11	Pa
Poisson's Ratio	0,3	
Bulk Modulus	1,6667E+11	Pa
Shear Modulus	7,6923E+10	Pa
Strain-Life Parameters		
Tensile Yield Strength	2,5E+08	Pa
Compressive Yield Strength	2,5E+08	Pa
Tensile Ultimate Strength	4,6E+08	Pa
Compressive Ultimate Strength	0	Pa

Figure 4.4: Engineering Data: Mechanical properties for the material *Structural Steel*

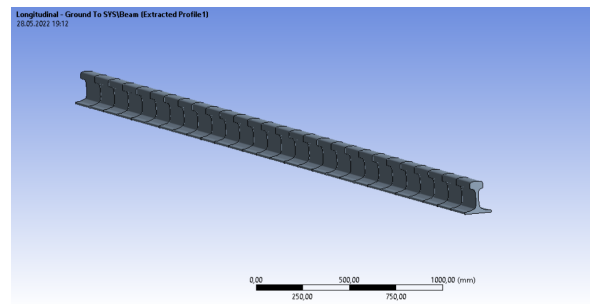
Mesh

Mesh, is a terminology profusely used in FEA. The mesh subdivides the given *computer aided design* (CAD) model into smaller sections referred to as "elements". Every element inherent a set of equations to be solved and to comply with neighbouring elements. If the mesh is incorrectly generated, the elements are unable act in accordance with the given boundary conditions and parameters. The element size is therefore a key parameter in order to obtain the most optimized solution.

The 'Details of Mesh' dialog box shows various settings for the meshing process.

Category	Property	Value
Display		
Defaults	Physics Preference	Mechanical
	Solver Preference	Mechanical APDL
	Element Order	Quadratic
	Element Size	250, mm
Sizing	Use Adaptive Sizi...	Yes
	Resolution	1
	Mesh Defeaturing	No
	Transition	Fast
	Span Angle Center	Coarse
	Initial Size Seed	Assembly
	Bounding Box Di...	7000, mm
	Average Surface ...	0, mm ²
	Minimum Edge L...	7000, mm

(a) List of details regarding the beam meshing



(b) Meshed rail beam with element size of 250 mm

Figure 4.5: Meshing data and meshed model

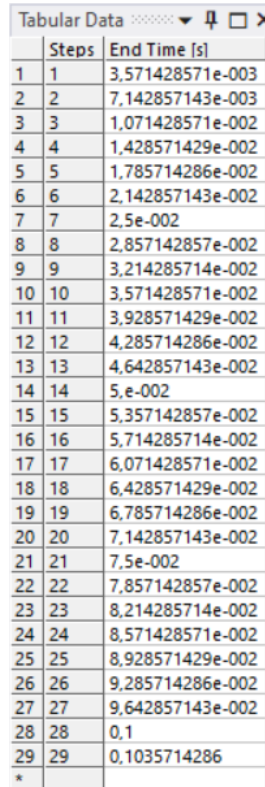
The element size of the mesh is, as seen in figure 4.5a, which results in a total amount of element of 28.

Time Segmentation

The train will be moving at a constant speed of 70 m/s and will cover the whole transition zone of 35 meter in 0.5 seconds. For the train to cover a 7 meter long rail it would take about 0.1 seconds. Dividing the time taken to transverse the beam on the 28 elements, it will give the time segments for each element.

$$\delta t = \frac{t_f}{n_{elements}} = \frac{0.1}{28} = 3.57142857142857 \times 10^{-3} \quad (4.6)$$

The time steps is inserted into a table in ANSYS, see figure 4.6.



	Steps	End Time [s]
1	1	3,571428571e-003
2	2	7,142857143e-003
3	3	1,071428571e-002
4	4	1,428571429e-002
5	5	1,785714286e-002
6	6	2,142857143e-002
7	7	2,5e-002
8	8	2,857142857e-002
9	9	3,214285714e-002
10	10	3,571428571e-002
11	11	3,928571429e-002
12	12	4,285714286e-002
13	13	4,642857143e-002
14	14	5,e-002
15	15	5,357142857e-002
16	16	5,714285714e-002
17	17	6,071428571e-002
18	18	6,428571429e-002
19	19	6,785714286e-002
20	20	7,142857143e-002
21	21	7,5e-002
22	22	7,857142857e-002
23	23	8,214285714e-002
24	24	8,571428571e-002
25	25	8,928571429e-002
26	26	9,285714286e-002
27	27	9,642857143e-002
28	28	0,1
29	29	0,1035714286
*		

Figure 4.6: List of time segments.

Connections

To simulate the elastic foundation, springs and dampers are connected underneath the beam as seen in figure 4.7.

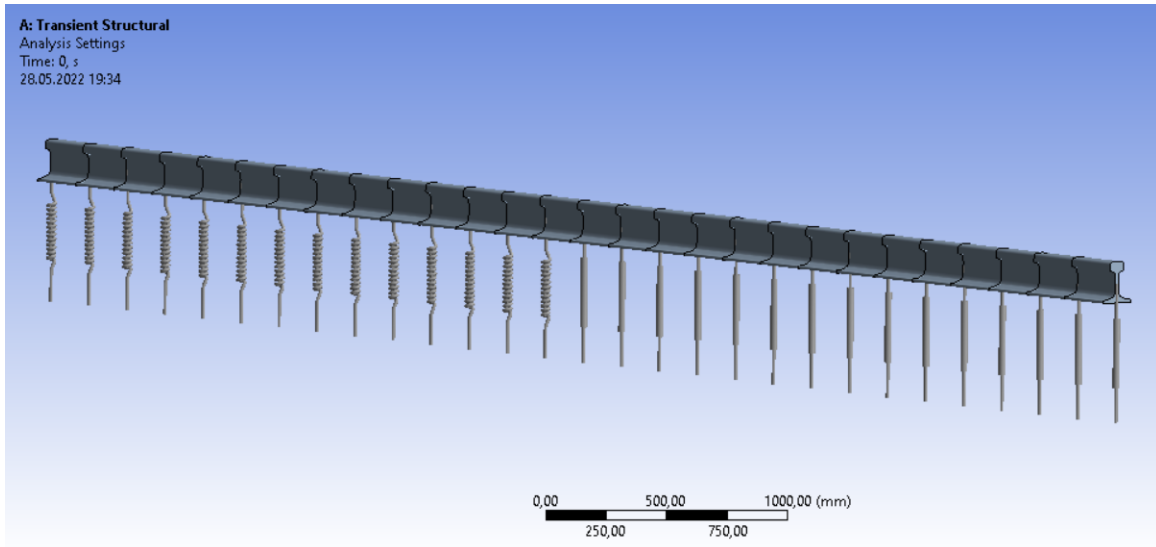


Figure 4.7: Springs and dampers connected underneath the rail beam.

The properties for the springs and dampers are the same used in the analytical solution, see figure 4.8.

Details of "Longitudinal - Ground To SYS\Beam (Extracted Profile1)"	
Graphics Properties	
Definition	
Type	Longitudinal
Spring Behavior	Both
<input type="checkbox"/> Longitudinal Stiffness	36500, N/mm
<input type="checkbox"/> Longitudinal Damping	7,89 N-s/mm
Preload	None
Suppressed	No
Spring Length	580,4624838 mm
Element APDL Name	

(a) Spring and damper details for the ballasted track.

Details of "Longitudinal - Ground To SYS\Beam (Extracted Profile1)"	
Graphics Properties	
Definition	
Type	Longitudinal
Spring Behavior	Both
<input type="checkbox"/> Longitudinal Stiffness	41700, N/mm
<input type="checkbox"/> Longitudinal Damping	0, N-s/mm
Preload	None
Suppressed	No
Spring Length	580,4624838 mm
Element APDL Name	

(b) Spring stiffness details for the ballastless track.

Figure 4.8: Details for the stiffness of the foundation.

Forces and Fixtures

The point load acts on each node consecutively in the negative z -direction of a value of 110363 N. The load is applied throughout the time step δt before moving on to the next node. Ideally, the beam should've been modeled to have an infinite length, this however is not possible. Instead, removing the load for the first and last four nodes to avoid unrealistic deflection at the end nodes. See figure 4.9 for the force-time graph. In addition to the load, standard earth gravity is also included in the analysis.

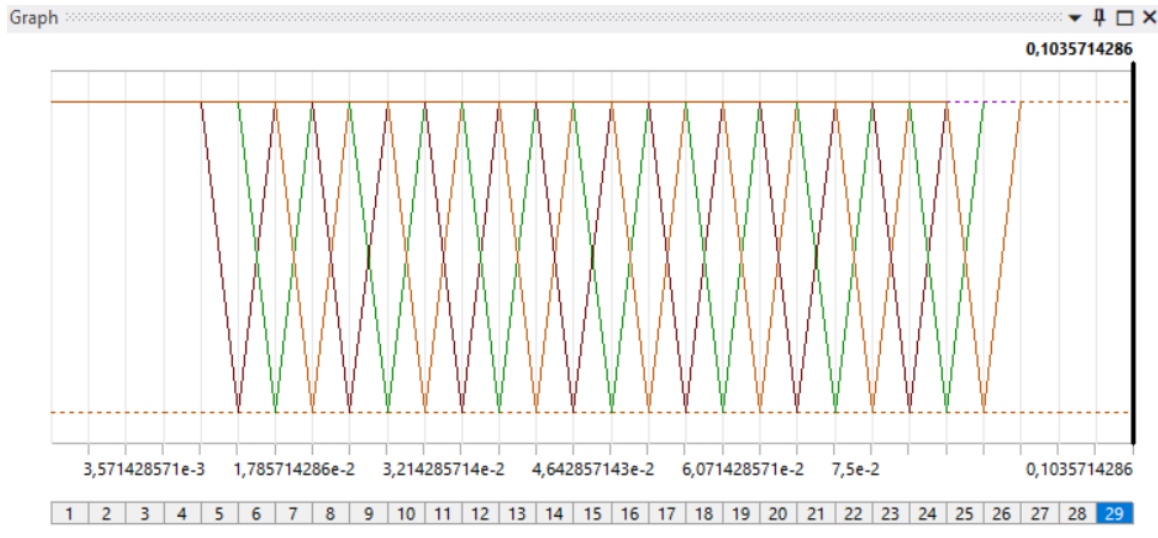


Figure 4.9: Force load vs time graph.

The analysis is limited to deflection in only the z -direction. Every element is therefore restricted to deflect in the x and y direction. Figure 4.10 shows the displacement restrictions.

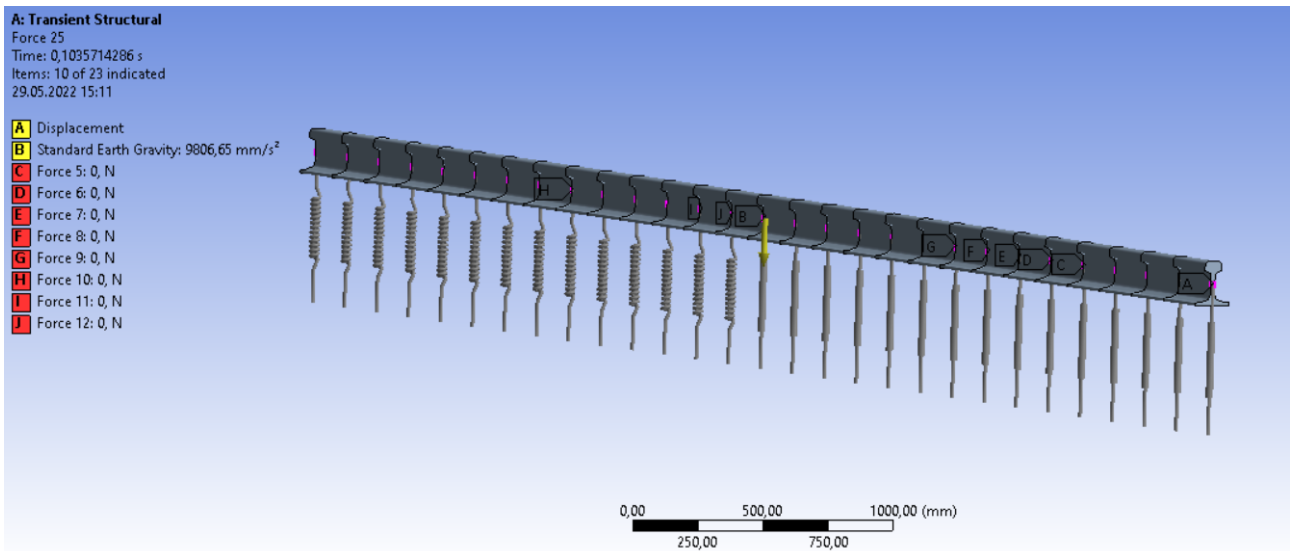


Figure 4.10: Displacement restriction fixture at each element.

Chapter 5

Results and Discussion

5.1 Analytical Results

MATLAB

The software MATLAB[24] was used to generate the deflection-, bending moment- and bending stress graphs. MATLAB is a matrix based programming language which can be used in computational analysis. The analytical formulation for the deflection was translated into MATLAB code to produce the curves shown in this chapter. The MATLAB code can be found in the Appendix H

Deflection

The solution to the differential equation shows how the deflection behaves when the train is moving with constant speed. The figure bellow depicts the maximum deflection at the load point for the ballasted section of the track.

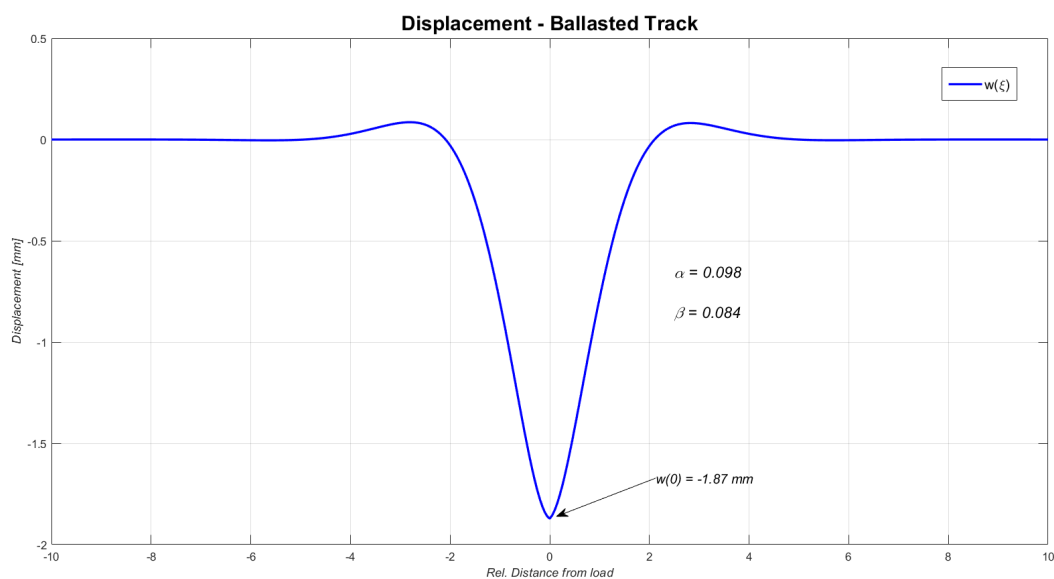


Figure 5.1: The graph depicts a wave which is the deflection of the rail as the train is moving along the track.

Figure 5.1 shows deflection with a velocity ratio $\alpha = 0.098$ and a damping ratio $\beta = 0.084$.

The maximum deflection will be $w(0) = -1.87$ mm.

For the ballastless section, the velocity ratio is $\alpha = 0.095$ and the damping ratio is $\beta = 0.0$. The deflection for this section results in a deflection of $w(0) = -1.75$.

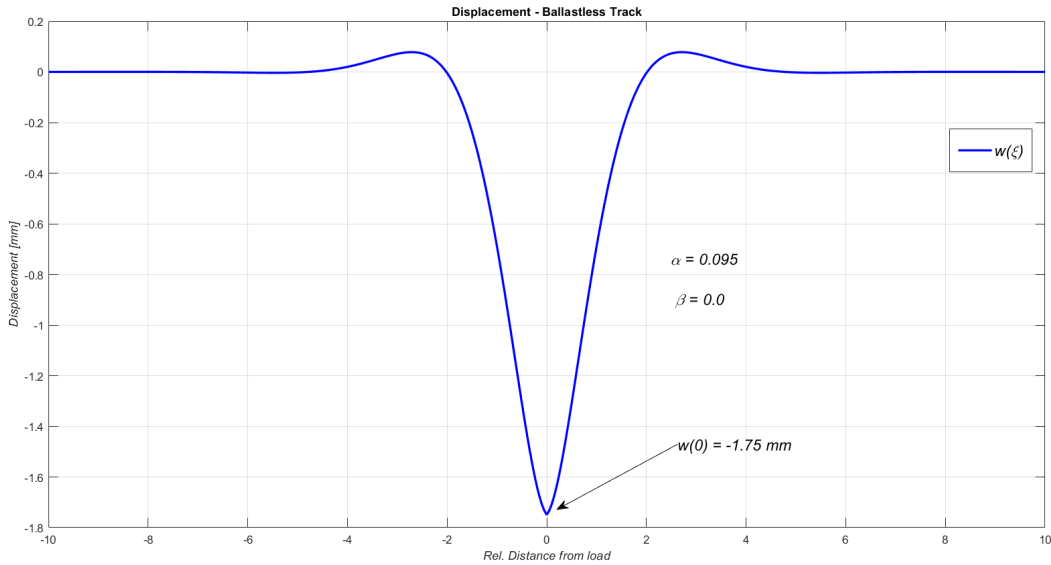


Figure 5.2: Deflection graph for the ballastless track.

The deflection function can further be used to analyse other important features such as; the bending moment in the rail and the bending stresses in the beam.

Analyzing the differences in deflection between the ballasted side and ballastless side the deflection varies only by 0.14 mm. According to Bane Nor, the limit to how much the deflection is allowed to vary between each change of elasticity is 0.5 mm [25]. Since the difference between the two are less than 0.5 mm than there might not be necessary to equalize this particular transition zone. However, as previously stated, due of the simplification from a two DoF to a single DoF system, the control of parameters have been weakened and the results may not be as accurate if a multi DoF system were implemented instead.

Bending Moment

The bending moment of the beam can be calculated using the double derivative of the deflection function:

$$M(\xi) = -\frac{d^2w(\xi)}{d\xi^2}EI \quad (5.1)$$

The bending moment is a measure on how the bending will affect the beam and is therefore an important function in structural analysis. The maximum and/or minimums of this function are key points of interest as they can be used in further analysis to point out the stresses in the beam.

Figure 5.3 depicts the bending moment graph of the rail at the ballasted section. The extremal value is shown to be $M(0) = 179$ Nm, and is located wherever the extremal of the deflection was.

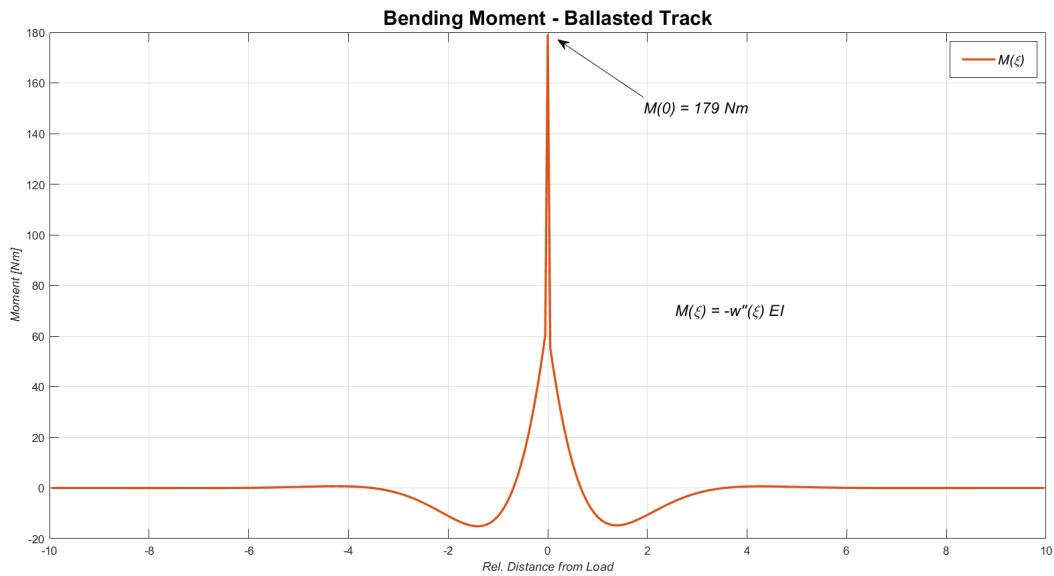


Figure 5.3: The graph illustrates how the bending moment in the rail behaves when the train moves along the rail in the ballasted section.

Figure 5.4 shows that the bending moment in the ballastless section $M(0) = 210 \text{ Nm}$.

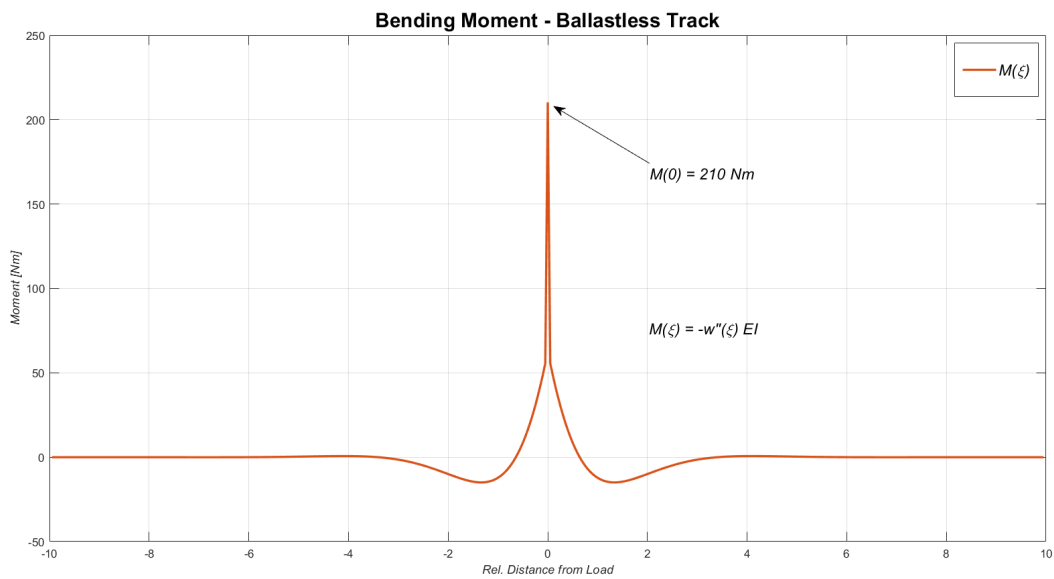


Figure 5.4: Bending moment graph for the ballastless track

Even though the deflection in the ballasted section is greater than the ballastless section, the bending moment in the ballastless side is greater.

Bending Stress

The load subjected onto the beam will induce bending stresses. As stated previously, the extremal point in which the bending moment occurs are key points of interest as these point are most likely to induce the greatest bending stresses. The function used to graph the bending stress is.

$$\sigma_b = \frac{M(\xi)c}{I} \quad (5.2)$$

Where, $M(\xi)$ is the bending moment function, c is the distance from either the head (top) of the rail or the foot (bottom) of the rail to the neutral axis, and I is the second area of inertia for the rail profile.

When bending occurs, there will be one side that are in compression and one side in tension. Since the load is being applied on top of the rail, the head of the rail beam will be in compression whilst the foot of the beam will be in tension. The parameter c will be positive at the head of the rail profile and negative at the foot. At the head of the rail $c = 91.05$ mm and at the foot $c = -80.95$ mm, see Appendix B for rail profile.

Figure 5.5 shows the bending stresses in both compression (in red) and tension (in blue) for the ballasted section of the track.

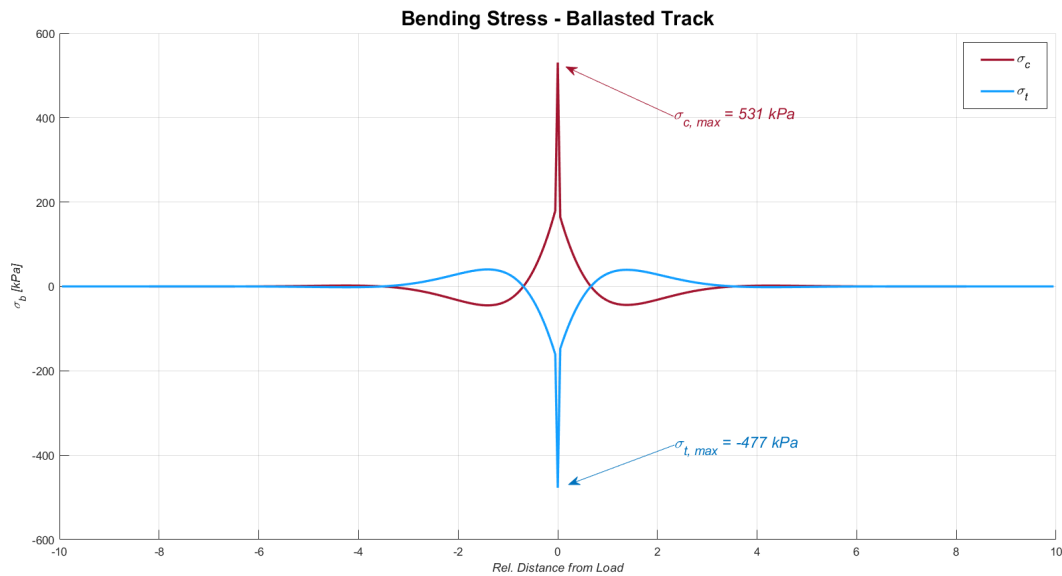


Figure 5.5: Bending stress in both compression and tension of the ballasted side of the track.

In the figure it is marked that bending stress in compression is $\sigma_{c,max} = 531$ kPa, while in tension it is $\sigma_{t,max} = -477$ kPa.

In the ballastless section, the bending stresses seem to be greater than in the ballasted section. Since the bending moment function for the the ballastless side is greater than the ballasted, it is not surprising that the bending stresses are greater as well. Figure 5.6 depicts the bending stresses for the ballastless side of the track.

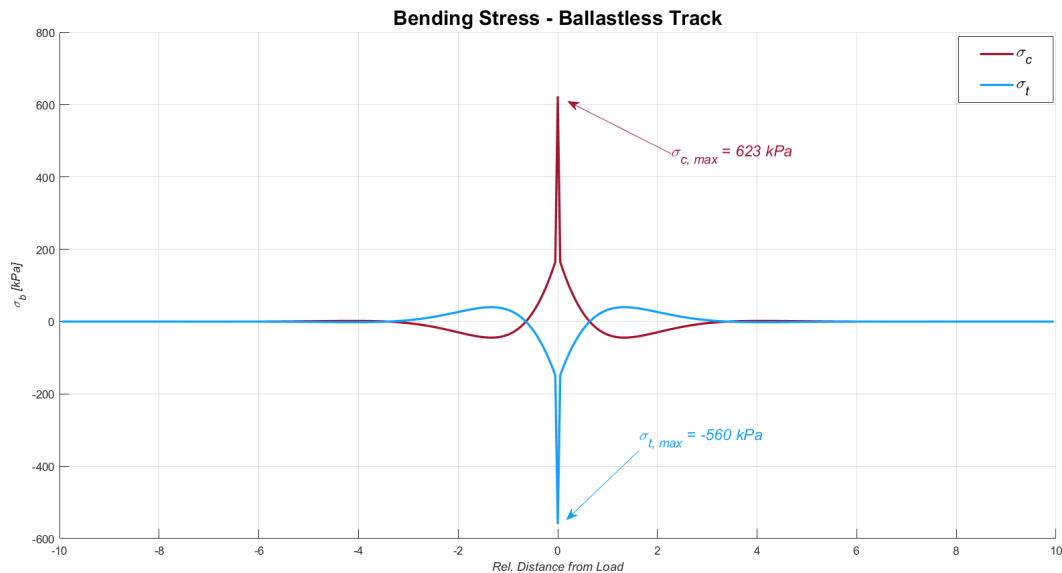


Figure 5.6: Bending stress σ_b for ballastless track

From the figure, the maximum stresses appear to be $\sigma_{c,max} = 623$ kPa, for rail compression and $\sigma_{t,max} = -560$ kPa in tension. The differences in stresses between the ballasted and the non-ballasted side are not negligible.

5.2 Numerical Results

Total Deformation

The total deformation shows a maximum deflection of 0.74 mm. The analytical solution showed a deflection of 1.87 mm in the ballasted track and 1.75 mm in the ballastless track. The numerical results does not match the analytical results, see figure 5.7 for the deflection of the rail.

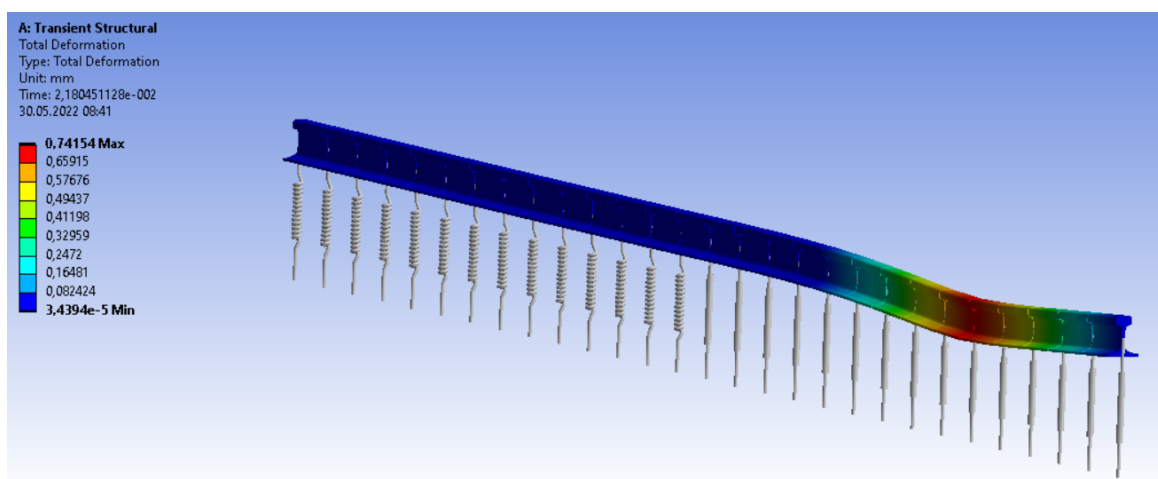


Figure 5.7: Total deformation of the rail beam at the transition point.

The error in the numerical analysis can be because of the elastic foundation not being continuous but rather discrete. However, the main objective of the numerical analysis were to animate the rail deflection. The animation is listed in the attachments.

Bending Moment

The numerical analysis calculated the bending moment to be 18.257 kNm which is about 5.3 times the maximum bending moment for the ballastless track in the analytical solution.

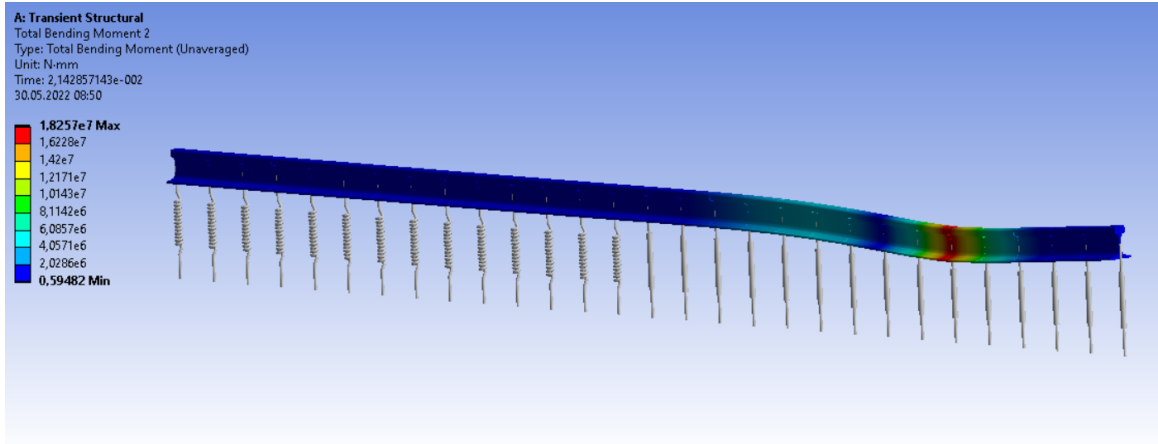


Figure 5.8: Maximum bending moment in the rail beam

Analysis Method	Deflection	Bending Moment	Bending Stress
<i>Analytical Ballast</i>	1.87 mm	179 Nm	531 KPa
<i>Analytical Non-Ballast</i>	1.75 mm	210 Nm	623 KPa
<i>Numerical Analysis</i>	0.74 mm	18.257 kNm	—

Table 5.1: Results from both analytical and numerical analysis

Extensive research and troubleshoots have been done to find an error yet, no clear explanation have been found.

It is uncertain why the differences in the results between the analytical and numerical are. A few guesses could be that ANSYS Worckbench calculates the problem differently than Mechanical APDL [26] which have been prone to happen in other problems. Error could have occurred during the modeling, however due to time limitations, remodelling will not be feasible. In addition, errors due to how the input-parameters relates to ANSYS’s interpretation and calculation of said parameters, could be the root cause. however, the inner workings of ANSYS is beyond the scope for this thesis.

In the analytical analysis, the calculation software MATLAB was used to calculate the differential equation and produce graphs. Translating the analytical mathematical calculation into MATLAB code is a potential source of error. Simulations of different lengths and loading have been done and can be found in the AppendixI.

5.3 Discussion

Considering that the damping ratio for the ballastless track were $\beta = 0.0$ may lead to the conclusion that introducing damping in the non-ballasted section can reduce the bending stress significantly and therefore reducing the rail impact degradation as well.

Gradually increasing the value of the damping ratio proved that the bending stress in the rail decreased. For a value for $\beta = 0.6$ seemed to match the bending stress to the ballasted track. The difference in the maximum bending stress reduced from 623 kPa down to 536.6 kPa.

To find a material with high damping properties it is possible to derive the material index for a spring. Recall that the critical damping is given by

$$c_{cr} = 2\sqrt{k\rho AL} \quad (5.3)$$

where k is the spring stiffness, ρ is the density, A is the area and L is the length of the material. The critical damping is dependant on the spring stiffness k and the density ρ , which means that whenever the spring stiffness or the density increases there will be an increase in the critical damping as well. Using Ashby's method for the spring material index, see Appendix D. The material index is given by

$$M = \frac{\sigma_y^2}{E\rho} \quad (5.4)$$

Where σ_y is the yield stress, E is the Young's modulus and ρ is the density. Taking the logarithm on both sides and solving for the yield stress, the equation for the slope becomes:

$$\ln \sigma_y = \frac{1}{2} \ln M + \frac{1}{2} \ln E\rho \quad (5.5)$$

Using the software Granta EduPack, a material chart can be generated, and plotting the line from Eq. (5.5), every material that are over or touches this line will have the wanted properties. In the software other limitations can be set such as; material cost, density and Young's modulus, yield stress, amongst many other properties. In this charth the material cost per kg was set to maximum 15 NOK.

Every material that are to the right of the green line are eliminated as well as all materials south from the blue line. The materials that are left will all have the properties viable for damping, these can be seen in figure 5.9.








-  EVA (Shore A95/D50, 12% vinyl acetate)
-  Natural rubber (15-42% carbon black)
-  Natural rubber (unreinforced)
-  Polyisoprene rubber (unreinforced)
-  Polyurethane rubber (unfilled)
-  PVC-elastomer (Shore A75)
-  Styrene butadiene rubber (SBR, 30% carbon black)

Figure 5.9: Names to all viable materials

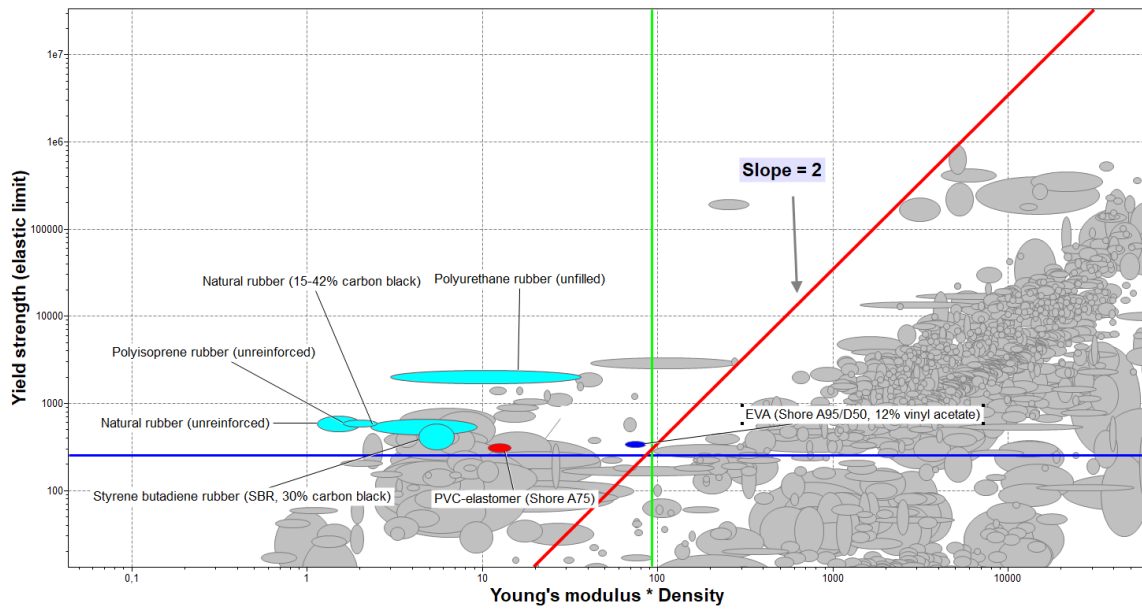


Figure 5.10: Materials viable for use. Red line is the material index line, green line is the density times Young’s modulus line and the blue is the yield stress line.

Material Name	ρ [kg/m^3]	E [MPa]	σ_y [MPa]	ε [%]	σ_N [MPa]
Ethylene Vinyl Acetate	930 - 940	70 - 90	18.0 - 19.0	730 - 770	13.5 - 14.3
Natural Rubber*	1020	2.1 - 8.4	20.0 - 27.0	385 - 690	8.0 - 10.8
Natural Rubber	930 - 970	1.2 - 2.1	21.0 - 28.0	600 - 780	8.4 - 11.2
Polyisoprene Rubber	930 - 970	1.7 - 2.6	23.0 - 25.8	500 - 760	9.2 - 10.3
Polyurethane Rubber	1190 - 1210	2.5 - 30	40.0 - 51.0	500 - 750	16.0 - 20.4
PVC-Elastomer	1210 - 1260	8.7 - 11.7	16.3 - 19.0	316 - 370	6.78 - 8.08
Styrene Butadiene	1130 - 1150	3.8 - 6.0	16.0 - 26.0	320 - 500	6.4 - 10.4

Table 5.2: List of materials

*Natural Rubber**: Reinforced Natural Rubber with 15 - 42% Carbon Black.

Based upon the formula for critical damping, the best suited material would be the material that has the highest density ρ and the highest fatigue strength at 10^7 cycles σ_N . That material would be: Polyurethane Rubber.

Another material that was not listed in the software but after researching, the material *Sorbothane* [27] was found. This material known to have an excellent damping coefficient, excellent shock absorbing and vibration isolation as well as having a very good temperature range of $-29\text{ }^\circ\text{C}$ to $72\text{ }^\circ\text{C}$ which is very suitable to Norwegian climate. Sorbothane is a viscoelastic polyurethane polyether-based thermoset material. Appendix G includes the data sheet for this material.

Chapter 6

Further Work and Ideas

At the start of this thesis, some promising ideas were discussed on how to approach the problem. The ideas seemed to lead to the right path, however some problems rose and due to some changes to the initial problem description, some of the ideas turned out to longer be applicable.

6.1 Lagrange's Equations

Lagrange's equations is a set of equations that is widely used in many fields of science; also in the field of structural dynamics. The equations are a reformulation of Newton's laws and are sometimes preferable to Newton's equation of motion.

Lagrange's equations are very powerful and are extremely useful in optimization problems. The motivation to use Lagrange's equations were to develop the equations of motion for the dynamical system. Another reason why Lagrange's equation were preferable over Newton's equation is that; the concept of vector and direction are no longer a necessity to keep track of, making Lagrange's equations much easier to work with.

Lagrange's equations are based upon **energy** systems; more specifically *the Lagrangian* [28]. The Lagrangian is typically noted $L = T - V$, where T is the kinetic energy and V is the potential energy of the system.

Figure 6.1 depicts a dynamical system where there are 2 DoF's present.

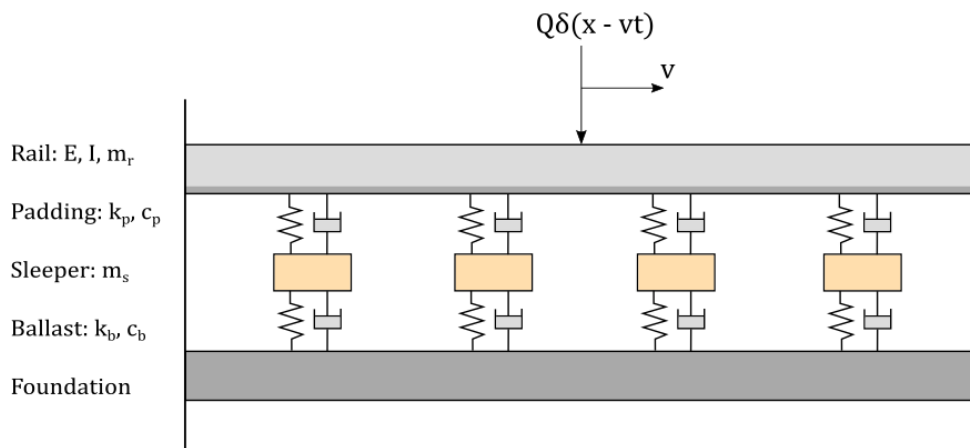


Figure 6.1: Ballasted railway track where there are 2 DoF's.

System of equations can be derived using Lagrange's equations which results in:

For $i = 1$

$$EIw_{1,xxxx} + m_r w_{1,tt} - k_p (w_1 - w_2) + c_p (w_{1,t} - w_{2,t}) = Q\delta(x - vt) \quad (6.1)$$

For $i = 2$

$$m_s w_{2,tt} - (k_p + k_b)(w_1 - w_2) + k_p w_1 - c_p (w_{1,t} - w_{2,t}) + c_b w_{2,t} = 0 \quad (6.2)$$

Where the subscript x and t corresponds to the partial derivative with respect to said subscript.

Since the problem stated in chapter 2 were reduced to a single degree of freedom problem, using Lagrange's equation to develop one equation of motion, this format will not be necessary. If however, a multi degree of freedom system were to be implemented, this method of developing the equations would be a viable option.

6.2 Fourier Transform Method

After developing the partial differential equation, a method to solve it were discussed. One method of solving it were to use the *method of separating of variables* [29]. It can be assumed that the transverse deflection $w(x, t)$ is a product of two separate functions such that:

$$w(x, t) = \phi(x)h(t) \quad (6.3)$$

Where, $\phi(x)$ is the modal deflections and $h(t)$ is an harmonic function of time t . Inserting Eq. (6.3) into Eq. (3.8), and incorporating that the external load is moving along the beam by using the *Dirac delta*:

$$EI \frac{d^4 \phi(x)}{dx^4} h(t) + \mu A \phi(x) \frac{d^2 h(t)}{dt^2} + c_{eq} \phi(x) \frac{dh(t)}{dt} + k_{eq} \phi(x) h(t) = Q\delta(x - vt) \quad (6.4)$$

Applying Fourier transform on each of the variables (using equations from Appendix (E)). The deflection function becomes:

$$\mathcal{F}(\mathcal{F}(w(x, t))) = \mathcal{F}(\widehat{W}(x, \omega)) = \widetilde{W}(\xi, \omega) \quad (6.5)$$

Eq. (6.4) reduces to an algebraic equation:

$$EI\xi^4 \widetilde{W}(\xi, \omega) - \mu A \omega^2 \widetilde{W}(\xi, \omega) + c_{eq} i \omega \widetilde{W}(\xi, \omega) + k_{eq} \widetilde{W}(\xi, \omega) = 2\pi Q \delta(\omega + v\xi) \quad (6.6)$$

By rearranging Eq. (6.6) and solving for the deflection in the frequency domain $\widetilde{W}(\xi, \omega)$ the equation becomes:

$$\widetilde{W}(\xi, \omega) = \frac{2\pi Q \delta(\omega + v\xi)}{EI\xi^4 - \mu A \omega^2 + c_{eq} i \omega + k_{eq}} \quad (6.7)$$

Simplifying Eq. (6.7) by factoring out $2\pi Q$ and $\frac{1}{EI}$. Furthermore let $\frac{\mu A}{EI} = \alpha$, $\frac{c_{eq}}{EI} = C$ and $\frac{k_{eq}}{EI} = K$.

$$\widetilde{W}(\xi, \omega) = \left(\frac{2\pi Q}{EI} \right) \left(\frac{\delta(\omega + v\xi)}{\xi^4 - \alpha\omega^2 + Ci\omega + K} \right) \quad (6.8)$$

To get the spatial and time deflection $w(x, t)$, an inverse Fourier transform in both ξ and ω must be calculated.

$$w(x, t) = \frac{Q}{2\pi EI} \int_{-\infty}^{\infty} \int_{-\infty}^{\infty} \frac{\delta(\omega + v\xi)}{\xi^4 - \alpha\omega^2 + Ci\omega + K} e^{i(\xi x + \omega t)} d\xi d\omega \quad (6.9)$$

This can yet be simplified by using Dirac-delta function's property such that:

$$w(x, t) = \frac{Q}{2\pi EI} \int_{-\infty}^{\infty} \frac{e^{i(\xi x + \omega t)}}{\xi^4 - \alpha\omega^2 + Ci\omega + K} d\xi \quad (6.10)$$

The solution to this have been influenced by another paper that discuss vibration of an elastic beam on a pasternak foundation under a moving load [30], which take use of double Fourier transform to solve the PDE. However, the solution is not an exact analytical solution as it requires numerical approximation to solve the integral. This method were therefore abandoned but kept as a method to solve the PDE.

6.3 Deriving the Euler — Lagrange Equation Using Calculus of Variation

Another approach were to make the problem into a optimization problem, were the idea were to minimize the energy used to deflect the rail. Euler - Lagrange Equation seemed to be a viable method as this equation have previously solved the infamous "*Brachistochrone Problem*", [31]. However, to utilize the Euler - Lagrange Equation, it must be derived. Using *Calculus of Variation* it is possible to derive it, [32].

Calculus of variation is a branch in mathematical analysis where the main objective is to find a function that optimizes a functional. For example; finding the shortest path between two points, or finding the shape of wire hanging between two posts.

As a parallel to calculus of one variable; when finding the extremal point of a function, the derivative is set equal to zero. The first derivative does not say anything about it being a maximum or minimum, though the sign of the second derivative will provide that information. The same procedure holds for calculation of variation when optimizing a path.

Suppose that there is a function $y(x)$ that minimizes some integral of a functional and is the optimal path who goes through the points (x_1, y_1) and (x_2, y_2) . To find all other paths, consider then an arbitrary, twice differentiable function; $\eta(x)$ that goes through the same two points; meaning that $\eta(x_1) = \eta(x_2) = 0$, but deviates from $y(x)$. This deviation can be described as $\varepsilon\eta(x)$.

By varying the parameter ε , all other paths can be found:

$$\bar{y}(x) = y(x) + \varepsilon\eta(x) \quad (6.11)$$

Where $\bar{y}(x)$ is every other path. Since every function is at least twice differentiable the derivative of equation (6.11) is:

$$\bar{y}'(x) = y'(x) + \varepsilon\eta'(x) \quad (6.12)$$

Using the commutative *Delta Operator* (or *Variation Operator*) to find the variation. Both y, \bar{y} and η and their derivatives are functions of the variable x , however, going forward these will not be explicitly written.

$$I = \int_{x_1}^{x_2} F(x, y, y')dx \quad (6.13)$$

$$\delta[I] = \int_{x_1}^{x_2} \delta[F(x, y, y')]dx \quad (6.14)$$

$$\bar{I} - I = \int_{x_1}^{x_2} F(x, \bar{y}, \bar{y}')dx - \int_{x_1}^{x_2} F(x, y, y')dx \quad (6.15)$$

In equation (6.15), I on the left hand side will cancel with the last term on the right hand side. The functional which is to be minimized:

$$\bar{I} = \int_{x_1}^{x_2} F(x, \bar{y}, \bar{y}')dx \quad (6.16)$$

Taking the derivative of the integral with respect to ε is needed to minimize the functional.

$$\frac{d\bar{I}}{d\varepsilon} = \int_{x_1}^{x_2} \frac{d}{d\varepsilon} (F(x, \bar{y}, \bar{y}'))dx \quad (6.17)$$

$$\frac{d\bar{I}}{d\varepsilon} = \int_{x_1}^{x_2} \left(\frac{\partial F}{\partial x} \frac{\partial x}{\partial \varepsilon} + \frac{\partial F}{\partial \bar{y}} \frac{\partial \bar{y}}{\partial \varepsilon} + \frac{\partial F}{\partial \bar{y}'} \frac{\partial \bar{y}'}{\partial \varepsilon} \right) dx \quad (6.18)$$

$$\left. \frac{d\bar{I}}{d\varepsilon} \right|_{\varepsilon=0} = \int_{x_1}^{x_2} \left(\frac{\partial F}{\partial \bar{y}} \eta + \frac{\partial F}{\partial \bar{y}'} \eta' \right) \Big|_{\varepsilon=0} dx \quad (6.19)$$

Evaluating $\varepsilon = 0 \rightarrow \frac{d\bar{I}}{d\varepsilon} = 0$ and according to equations (6.11) and (6.12), all paths will converge to the optimal path, which means that $\bar{y} = y$ and $\bar{y}' = y'$.

$$\int_{x_1}^{x_2} \left(\frac{\partial F}{\partial y} \eta + \frac{\partial F}{\partial y'} \eta' \right) dx = 0 \quad (6.20)$$

Equation (6.20) is the first variation ($\delta^{(1)}$) and is a weak form because it's containing a derivative of the arbitrary function $\eta'(x)$. To make equation (6.20) a strong form, the last term can be integrated by parts. That will result in.

$$\left. \frac{\partial F}{\partial y'} \eta \right|_{x_1}^{x_2} + \int_{x_1}^{x_2} \left(\frac{\partial F}{\partial y} - \frac{d}{dx} \left(\frac{\partial F}{\partial y'} \right) \right) \eta dx = 0 \quad (6.21)$$

Because η is arbitrary it is appropriate to apply — Fundamental Lemma of Calculus of Variation. The Euler — Lagrange equation:

$$\frac{\partial F}{\partial y} - \frac{d}{dx} \left(\frac{\partial F}{\partial y'} \right) = 0 \quad (6.22)$$

The idea of using the Euler - Lagrange equation to minimize the deflection energy were abandoned because of another idea presented itself which seemed to be somewhat easier to solve. That idea became the main focus in this paper and were discussed in details in chapter 2. Nevertheless, the Euler - Lagrange minimization energy method could be an interesting method to further develop as research on this topic is scarce.

6.4 Equalization of Elasticity

Modeling the transition zone can be done if the spring stiffness and the damping both are functions position. Recall that for the ballasted side, the spring stiffness and damping coefficients comes from the padding and the ballast, where as in the non-ballasted side, only the spring stiffness from the padding contributes.

When the train moves closer towards the non-ballasted side, the stiffness will at some location x change from one to the other. Therefore, letting the spring stiffness and the damping be a function of position, will result in a function that can vary its stiffness according to its position. The stiffness at one position to another can be described in the following way:

$$k_n(x) = \begin{cases} k_1, & \text{for } x \leq x_0 \\ k_2, & \text{for } x > x_0 \end{cases} \quad (6.23)$$

The same can be said for the damping:

$$c_n(x) = \begin{cases} c_1, & \text{for } x \leq x_0 \\ c_2, & \text{for } x > x_0 \end{cases} \quad (6.24)$$

To be able to utilize that the stiffness and the damping changes dependant on the position, the stiffness and damping values must be updated to fit the new condition. To update the spring stiffness and damping coefficients the *Unit step-function* or *Heaviside-function* can be multiplied with the stiffness and damping function. The Heaviside-function is defines as:

$$u(x) = \begin{cases} 0, & \text{for } x \leq x_0 \\ 1, & \text{for } x > x_0 \end{cases} \quad (6.25)$$

The spring function can therefore be written as a product of stiffness and Heaviside-function, $K_n(x)$:

$$K_n(x) = \sum_{i=0}^n k_i u(x - x_i) \quad (6.26)$$

And for damping, $C_n(x)$:

$$C_n(x) = \sum_{i=0}^n c_i u(x - x_i) \quad (6.27)$$

Where n is the number of elastic changes throughout the transition zone. The idea here is to equalize the transition zone by increasing the stiffness and damping in the padding by increasing the number of spring stiffness and damping functions $k_n(x)$ and $c_n(x)$ by letting $n > 2$.

The equation of motion would look like this:

$$EI \frac{\partial^4 w}{\partial x^4} + \mu A \frac{\partial^2 w}{\partial t^2} + \sum_{i=0}^n c_i u(x - x_i) \frac{\partial w}{\partial t} + \sum_{i=0}^n k_i u(x - x_i) w = Q \delta(x - vt) \quad (6.28)$$

Although this idea is original, it was ultimately abandoned because of the time limitation of this thesis. Time taken to prove that this method would work could exceed the time limitation and were deemed too risky to pursue. This method could be very interesting to follow up on for further development.

Chapter 7

Conclusion

An explicit analytical solution for the deflection of a beam resting on spring and damper foundation with a moving load, have been calculated for both ballasted track and non-ballasted track. Because the problem is a single degree of freedom system, the method used to develop the equation of motion was to apply Newton's laws of motion. Hence, a fourth order partial differential equation was obtained which was solved using a technique called change of coordinates. When changing the coordinate system we will instead obtain a coordinate system following the train's velocity. This method reduced the equation to a fourth order ordinary differential equation.

The solution to the equation produces a deflection curve which depicts how the deflection in the rail behaves under certain velocity ratios and damping ratios. Depending on the different foundation; padding material, ballast, etc, and velocities the ratios will vary. When analyzing the the deflection between the two different sides of a transition zone, the results revealed that the ballasted side's deflection was $w(0) = -1.87$ mm and the non-ballasted side's deflection was $w(0) = -1.75$ mm. According to technical standards, the maximum allowable deflection in between changes of elasticity is 0.5 mm. Since the difference in deflection were 0.14 mm, an increase in stiffness during this particular transition zone might not be necessary. However if a multi degree of freedom system were implemented the results could vary because of the limited control of the parameters when only implementing a single degree of freedom model. The bending stress, on the other hand, revealed that the ballastless track with no damping is subjected to a significantly higher stress of 623 kPa relative to the ballasted track which is subjected to 531 kPa. To reduce the track degradation, introducing some damping into the ballastless track will reduce the bending stress. Applying Ashy's method of determining the material index of elastic springs, we could generate a material chart that excluded less optimal materials for damping. The exclusion eliminated all but 7 materials where one stood out as the best: Polyurethane Rubber. Another material was found after some research called Sorbothane which also have excellent damping qualities. Other qualities this material had was shock absorption, vibration reducing technology and a temperature range of $-29^{\circ}\text{C} - 72^{\circ}\text{C}$ which is very suitable for harsher climate such as Norway's.

Developing a mathematical model for a train **in** a transition zone on the other hand, demands more time. Some ideas presented in the previously chapter may provide a solution if the ideas were to be implemented. Nevertheless, a finite element method were used to show an animation of the rail when a moving load was applied. The animation was made using a tool called transient structural which the computer software ANSYS is equipped with. Based upon the rail profile used by Bane Nor in the Follo line project, the same rail beam was design in the modelling software. The beam was extruded to a length of 7 meters, even though the transition

zone's length is 35 meters, just a segment of that would be enough. The mesh of the beam had an element length of 250 mm, which means that the beam have a total element count of 28.

The train will travel the 7 meters long beam in 0.1 seconds hence, the force applied to each node lasts for $\frac{1}{280}$ seconds. The results from this analysis showed that the maximum deflection was 0.74 mm which didn't match the analytical deflection. The bending moment as well didn't match between the two methods. This must therefore be analyzed further and in more detail.

Bibliography

- [1] A. C. Lamprea-Pineda, D. P. Connolly, and M. F. Hussein, “Beams on elastic foundations – A review of railway applications and solutions,” *Transportation Geotechnics*, vol. 33, p. 100696, 3 2022.
- [2] Jernbanekompetanse, “Sporets komponenter.” https://jernbanekompetanse.no/wiki/Sporets_komponenter.
- [3] Rouhollah Basirat, “Schematic showing a transition zone.” <https://www.researchgate.net/profile/Rouhollah-Basirat/publication/316986138/figure/fig1/AS:494851332337664@1494993159656/Schematic-showing-a-transition-zone.png>, May 2017.
- [4] Bane Nor, “Follo line.” <https://www.banenor.no/Prosjekter/prosjekter/follobanen/>, 2021.
- [5] Yu. L. and Chan. T., “Moving force identification from bending moment responses of bridge.” https://www.researchgate.net/publication/27472461_Moving_force_identification_from_bending_moment_responses_of_bridge, 2002.
- [6] T. Regelverk, “Rail profile 60e1.” https://trv.banenor.no/w/index.php?title=Fil:JD530_06b_fig004.png&filetimestamp=20101122084937&,.
- [7] Ashby. M. F., “Material selection in mechanical design.” <https://www.akademika.no/9780081005996/teknologi/maskin-og-mekanikk/materials-selection-mechanical-design>, 2016.
- [8] T. Regelverk, “Permissible speed and axle load for superstructure class.” https://trv.banenor.no/wiki/Overbygning/Prosjektering/Generelle_tekniske_krav#Overbygningsklasser,.
- [9] Jernbanekompetanse, “Ballast.” https://jernbanekompetanse.no/wiki/Sporets_komponenter/Ballast.
- [10] getzner, “Optimisation of transition zones.” <https://www.getzner.com/en/subject-areas/transition-zones>.
- [11] Bane Nor, “Follobanen.” <https://www.banenor.no/Prosjekter/prosjekter/follobanen/>.
- [12] S. S. Rao, “Mechanical vibrations.”
- [13] Henri J. Nussbaumer, “Fast fourier transform and convolution algorithms.” https://link.springer.com/chapter/10.1007/978-3-662-00551-4_4.

- [14] B. Indraratna, M. Babar Sajjad, T. Ngo, A. Gomes Correia, and R. Kelly, “Improved performance of ballasted tracks at transition zones: A review of experimental and modelling approaches,” 12 2019.
- [15] L. Izvolt, J. Harusinec, and M. Smalo, “Optimisation of transition areas between ballastless track and ballasted track in the area of the tunnel turecky vrch,” *Communications - Scientific Letters of the University of Zilina*, vol. 20, no. 3, pp. 67–76, 2018.
- [16] T. Xin, Y. Ding, P. Wang, and L. Gao, “Application of rubber mats in transition zone between two different slab tracks in high-speed railway,” *Construction and Building Materials*, vol. 243, 5 2020.
- [17] C. Ngamkhanong, Q. Y. Ming, T. Li, and S. Kaewunruen, “Dynamic train-track interactions over railway track stiffness transition zones using baseplate fastening systems,” *Engineering Failure Analysis*, vol. 118, 12 2020.
- [18] C. Esveld, *Modern Railway Track*. Groenwal 25 - NL-5301 JJ Zaltbommel - The Netherlands: MRT-Productions, digital edition 3.8 ed., 2001.
- [19] Standard Norge, “Railway applications Ballastless track system Part 2: System design, subsystems and components,” 11 2017.
- [20] Rail One, “Rheda 2000 ballastless track system.” https://www.railone.com/fileadmin/daten/05-presse-medien/downloads/broschueren/en/Rheda2000_EN_2011_ebook.pdf.
- [21] Leon van Dommelen, “Partial differential equation.” https://web1.eng.famu.fsu.edu/~dommelen/pdes/style_a/cc.html.
- [22] Sun. C. T., “Mechanics of aircraft structures,” 2006.
- [23] J. S. ”Archer, ““consistent matrix formulations for structural analysis using finite-element techniques”,” ”*AIAA Journal*”, vol. 3, pp. 1910—1918, 1965.
- [24] MathWorks, “Matlab.” https://se.mathworks.com/products/matlab.html?s_tid=hp_products_matlab.
- [25] Teknisk Regelverk, “Teknisk regelverk.” <https://trv.banenor.no/wiki/Forside>.
- [26] ANSYS, “Introduction to ansys mechanical apdl.” <https://www.ansys.com/training-center/course-catalog/structures/introduction-to-ansys-mechanical-apdl>.
- [27] Sorbothane, “Sorbothane overview.” <https://www.sorbothane.com/material-properties.aspx>, 2022.
- [28] Hand, L. N. and Finch, J. D., “Analytical mechanics,” 13 November 1998.
- [29] Paul Dawkins, “Separation of variables.” <https://tutorial.math.lamar.edu/classes/de/SeparationofVariables.aspx1>, 2003 - 2022.
- [30] Adair, Desmond and Nagimova, Aigul, “Vibration of an elastic beam on a pasternak foundation under a moving load.” 2019.
- [31] Encyclopedia of Mathematics, “Brachistochrone.” <http://encyclopediaofmath.org/index.php?title=Brachistochrone&oldid=31993>, 2019.
- [32] Wikipedia, “Calculus of variations.” https://en.wikipedia.org/wiki/Calculus_of_variations.

Appendix A

Tables

Superstructure Class	Carriages in passenger trains		Motor vehicle set		Freight trains / Work machines		
	Nominal axle load (tons)	Max velocity (km/h)	Nominal axle load (tons)	Max velocity (km/h)	Nominal axle load (tons)	Max velocity (km/h)	Max velocity bogies approved acc. EN 14363 (km/h)
a	16	90	16	90	22,5	30	30
					16,5	70	70
b	18	100	18	100	22,5	30	30
					20,5	70	70
					18	80	80
c	18	160	20,5	130	22,5	80	90
			18	160	20,5	90	100
			—	—	18	100	110
c+	18	160	20,5	160	241	50	50
					22,5	90	100
					20,5	100	110
					18	110	120
d	18	230	20,5	160	25	70	70
			20	200	22,5	100	120
			18	250	18	110	120
			17	300	—	—	—
Ofot Line	18	130	20,5	130	31	50	50
					22,5	70	70
Ofot Line 35t	18	130	20,5	130	35	50	50
					22,5	70	70

Table A.1: Permitted velocity and maximum axle load for superstructure classes, [8].

Superstructure Class	Rail Profile	Max Sleeper Distance
a	35,7 kg	730 mm
	S41	750 mm
	49E1	750 mm
b	35,7 kg	610 mm
	NSB40	610 mm
	S41	660 mm
c	49E1	660 mm
	54E3	660 mm
	54E2	650 mm
	54E1	670 mm
	S64	750 mm
c+	49E1	600 mm
	54E3	600 mm
	54E1	600 mm
	54E2	600 mm
d	60E1	600 mm
Ofot Line	54E4	520 mm
	60E2	520 mm
Ofot Line 35t	60E2	520 mm

Table A.2: Rail profile with associated maximum sleeper distance for superstructure classes, [8].

Appendix C

Vipa DFC

PANDROL

VIPA DFC



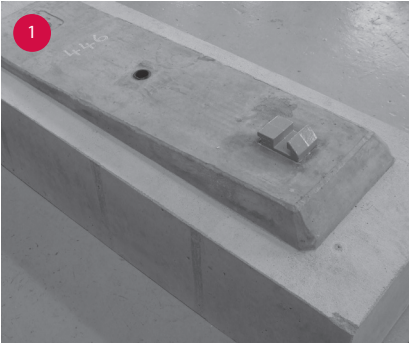
PRODUCT INFORMATION



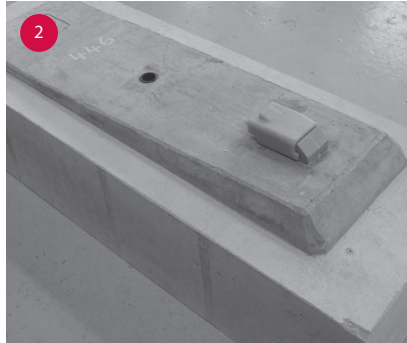


PRE-ASSEMBLY PROCESS

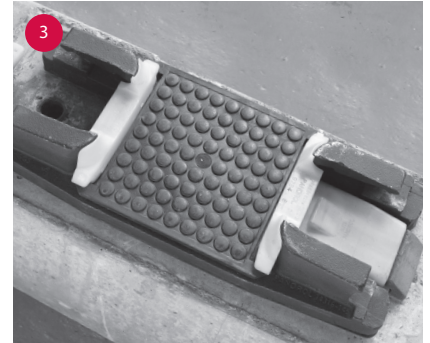
Installation into parked position



The sleeper is supplied with a cast-in SGI iron shoulder on the field side and a cast-in plastic insert on the gauge side of the rail seat.



A field-side clamp is positioned on the field-side SGI shoulder.



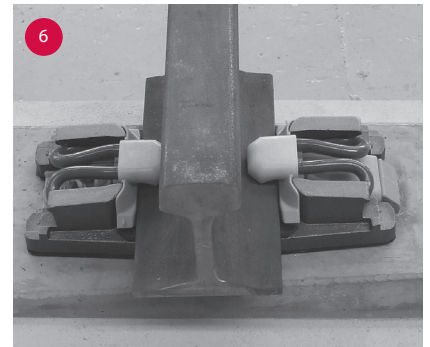
The baseplate (with side-post insulators and baseplate pad already in position beneath it) is slid into engagement with the field-side clamp.



The gauge-side clamp is positioned and bolted down.



Pandrol Fastclip clips are installed into the parked position. Assembly are normally delivered to site in this configuration.



Once the sleepers are placed and the rail has been threaded, clips are driven from the parked to the working position.

FEATURES OF ASSEMBLY

LATERAL LOAD TRANSFER

PANDROL VIPA DFC provides low track stiffness and high lateral loading resistance. This is made possible by a cast-in shoulder, which transfers lateral loads from the train through the baseplate and into the concrete. The energy transfer is similar to that of cast-in shoulders on concrete sleepers in conventional ballasted tracks.

MANY APPLICATIONS

The system features an adjustable indirect baseplate type that is ideal for installation on pre-cast blocks, sleepers and slabs. It can also be installed by wet-pour, top-down methods. Track and

structure interaction is accommodated by low-toe load variants.

FULLY PRE-ASSEMBLED

PANDROL VIPA DFC baseplates can be delivered to track sites fully pre-assembled on the pre-cast sleeper, block or slab.

HIGHLY ADJUSTABLE

Lateral adjustment of +/-5 mm per rail seat is facilitated by exchanging the side-post insulators. Vertical adjustment of +20 mm, in 1 mm increments, is facilitated by exchanging the field-side clamp and shimming under the baseplate using simple flat shims.

Greater levels of vertical adjustment are also possible, depending on operating conditions.

LOW STATIC STIFFNESS

Resilient rail and baseplate pads enable VIPA DFC to meet demanding stiffness requirements. The system provides static stiffness as low as 12.5 kN/mm for LRT systems, 15-20 kN/mm for metro systems and 20-25 kN/mm for main line slab tracks (depending on materials used).

PANDROL

VIPA DFC

- Suitable for use on non-ballasted (slab) tracks
- Suitable for top down construction
- Optimised for use on pre-cast blocks, sleepers and slabs

Application data (Standard products – special variants may differ)				
Rail Inclination	Provided in the concrete as required			
Typical Applications	LRT/Metro, general main line, high speed non ballasted tracks			
Clip Type	PANDROL FASTCLIP FC1501, FC1504			
EN 13481-5 Track Category	Cat A	Cat B	Cat C	Cat D
Maximum Axle Load*	130 kN	180 kN	260 kN	260 kN
Minimum Curve Radius*	40 m	80 m	150 m	400 m

* For special applications consult PANDROL

Typical performance data* As identified by Track Category EN 13481-1					
	Cat A	Cat B	Cat C/D	Test method	Remarks
Assembly static stiffness	12.5-17.5 kN/mm	15-20 kN/mm	20-25 kN/mm	EN 13146-9:2011	Dependent upon pad selection
Assembly dynamic stiffness	17.5-22.5 kN/mm	20-25 kN/mm	25-30 kN/mm	EN 13146-9:2011	
Electrical insulation	>10 kΩ				
Nominal toe load	1000 kgf				
Clamping force	>16 kN			EN 13146-7:2012	
Creep resistance	>9 kN			EN 13146-1:2012	
Lateral adjustment	+/- 5 mm				
Vertical adjustment	+ 20 mm				

COMPLIANCE WITH STANDARDS:

PANDROL VIPA DFC has been tested against and meets the EN 13481-5:2012 'Fastening Systems for Slab Tracks' standards. It also meets European High Speed TSI (Technical Standards for Interoperability) requirements.

NOTE:

PANDROL is a provider of innovative custom rail fastenings. Data in this document indicates typical performance. Actual performance is dependent on a range of external factors. Please contact us to discuss how PANDROL can tailor products to suit local operating conditions and specific requirements. Technical information in this document was correct at time of printing. Improvements may since have been introduced as a result of our continuous research and development programmes.

ISSUE 3 2015

PANDROL TRACK SYSTEMS

63 Station Road
 Addlestone, Surrey
 KT15 2AR
 England

Telephone: **+44 (0)1932 834500**
 e-Mail: **info@pandrol.com**
 Website: **www.pandrol.com**



Appendix D

Material Index

Table B3 Strength-limited design: springs, hinges etc. for maximum performance*

<i>Function and constraints</i> ^{*‡}	<i>Maximize</i> [†]
Springs	
maximum stored elastic energy per unit volume; no failure	σ_f^2/E
maximum stored elastic energy per unit mass; no failure	$\sigma_f^2/E\rho$

Figure D.1: Maximum stored elastic energy in springs [7]

Appendix E

Fourier Transform

$$\hat{f}(x, \omega) = \int_{-\infty}^{\infty} f(x, t) e^{-i\omega t} dt \quad (\text{E.1})$$

$$f(x, t) = \frac{1}{2\pi} \int_{-\infty}^{\infty} \hat{f}(x, \omega) e^{i\omega t} d\omega \quad (\text{E.2})$$

$$\tilde{f}(\xi, \omega) = \int_{-\infty}^{\infty} \hat{f}(x, \omega) e^{-ix\xi} dx \quad (\text{E.3})$$

$$\hat{f}(x, \omega) = \frac{1}{2\pi} \int_{-\infty}^{\infty} \tilde{f}(\xi, \omega) e^{ix\xi} d\xi \quad (\text{E.4})$$

Appendix F

Master's Thesis Topic

University of Tromsø – The Arctic University of Norway
Faculty of Engineering Science and Technology
Department of Computer Science and Computational Engineering

Master of Science

**Master thesis topic: Design and modelling of transition structure
between ballasted and non-ballasted railway track**

**(Design og modellering av overgangssone mellom ballastfritt spor og
spor med ballast på jernbanen)**

Candidate name Joachim Jørgensen Ågotnes
Master thesis in Engineering Design spring 2022

Problem description

Railway systems can be of ballast type or non-ballast type. The main railway system in Norway has been of the ballast type. Non-ballast structures are used in areas where for instance ballast is not wanted for instance in bridges, in tunnels with limited heights and possibilities to perform maintenance. Also, high-speed railways are often made of non-ballasted tracks. The combination of ballasted and non-ballasted tracks in different parts of the railway will cause some challenges that must be solved. For instance, in the transition area, the different flexural stiffness of the two types of track design is of great importance. In order to make the transition as smooth as possible the mechanical properties of that part of the railroad must be designed in a best possible way. The mathematical models that describe this transition area is of great interest to explore and develop in order to be able to design a best possible transition system. In this way, the wear of the track and trains can be as low as possible, at a minimum need for maintenance. The elasticity and dynamical properties of the transition area are of special interest and will be influenced on e.g. type of rails, sleepers, slabs and ballast system. The overall (static and dynamic) behavior of the track system must be according to the requirements of BaneNor (and Jernbaneverket) in Norway. The problem formulation is originally developed by BaneNor and refined and described in cooperation between UiT and BaneNor.

The work shall include:

1. **A literature study** both in terms of finding state-of-the-art for these types of structures and solutions in the market and potential competitors, as well as literature that is necessary to solve the problem (regulations, standards for materials, algorithms etc.).
2. **Establishment of some case studies** including specifications (i.e., loading and boundary conditions, physical conditions, requirements for stiffness, strength, weight, materials, temperatures).
3. **The main work will be on mathematical modelling, analytical and numerical analysis of the system included some case studies. A systematic material selection process may be used if it is relevant for the new design of (parts of) the system .**
4. **Suggestions** for future work and description of remaining work.

The solution of the task should be based on typical engineering design methods and areas of study for the Master Program Engineering Design at UiT – campus Narvik.

General information

This master thesis should include:

- ✳ Preliminary work/literature study related to actual topic
 - A state-of-the-art investigation

- An analysis of requirement specifications, definitions, design requirements, given standards or norms, guidelines, and practical experience etc.
 - Description concerning limitations and size of the task/project
 - Estimated time schedule for the project/ thesis
-
- ✳ Mathematical modelling of the system
 - ✳ Selection & investigation of relevant materials and products
 - ✳ Development (creating a model or model concept)
 - ✳ Experimental work (if planned in the preliminary work/literature study part)
 - ✳ Suggestion for future work/development
 - ✳ An oral presentation of the thesis/work will be performed. BaneNor will be invited to the (digital) presentation

Limitations of the task/project

There may be information in the report that may not be open, and if so, the report should be restricted. This will be considered before the candidate submits the thesis.

Preliminary work/literature study

After the task description has been distributed to the candidate a preliminary study should be completed within 4 weeks. It should include bullet points 1 and 2 in “The work shall include”, and a plan of the progress. The preliminary study may be submitted as a separate report or “natural” incorporated in the main thesis report. A plan of progress and a deviation report (gap report) can be added as an appendix to the thesis.

In any case the preliminary study report/part must be accepted by the supervisor before the student can continue with the rest of the master thesis. In the evaluation of this thesis emphasis will be placed on the thorough documentation of the work performed.

Reporting requirements

The thesis should be submitted as a research report and must include the following parts: Abstract, Introduction, Material & Methods, Results & Discussion, Conclusions, Acknowledgements, Bibliography, References and Appendices. Choices should be well documented with evidence, references, or logical arguments.

The candidate should in this thesis strive to make the report survey-able, testable, accessible, well written, and documented.

Materials which are developed during the project (thesis) such as software/codes or physical equipment are a part of this paper (thesis). Documentation for correct use of such information should be added, as far as possible, to this paper (thesis).

The text for this task must be added as an appendix to the report (thesis).

The report (Abstract, Introduction, Material & Methods, Results & Discussion, Conclusions, Acknowledgements, Bibliography, References) should not exceed 50 pages. Any additional material should be included in the appendix.

General project requirements

If the tasks or the problems are performed in close cooperation with an external company, the candidate should follow the guidelines or other directives given by the management of the company.

The candidate does not have the authority to enter or access external companies' information system, production equipment or likewise. If such should be necessary for solving the task in a satisfactory way a detailed permission should be given by the management in the company before any action are made.

Any travel cost, printing and phone cost must be covered by the candidate themselves, if and only if, this is not covered by an agreement between the candidate and the management in the enterprises.

If the candidate enters some unexpected problems or challenges during the work with the tasks and these will cause changes to the work plan, it should be addressed to the supervisor at the UiT Campus Narvik or the person which is responsible, without any delay in time.

Submission requirements

This thesis should result in a final report with an electronic copy of the report included appendices and necessary software codes, simulations, and calculations. The final report with its appendices will be the basis for the evaluation and grading of the thesis. The report with all materials should be delivered in an electronic format. The report should be in PDF format while the rest of the material should be bundled in ZIP file. A standard front page, which can be found on the UiT Campus Narvik internet site, should be used. Otherwise, refer to the "General guidelines for thesis" and the subject description for master thesis.

The final report with its appendices should be submitted no later than the decided final date. The final report should be delivered/ submitted/ uploaded to WISEflow.

Date of distributing the task: 11.01.2022

Date for submission (deadline): xx.x.2022

Master thesis task for
Candidate name Joachim Jørgensen Ågotnes

Contact information

Supervisors at the UiT Narvik

Professor Annette Meidell

annette.meidell@uit.no

Professor Dag Lukkassen

dag.lukkassen@uit.no

Førsteamanuensis Guy Mauseth

guy.b.mauseth@uit.no

Candidates contact information

Joachim Jørgensen Ågotnes

jaa055@uit.no

Appendix G

Material — Sorbothane



**Material Properties
of Sorbothane®**

EFFECTIVE 8/17/21

PROPERTY	DUROMETER (Shore 00)			UNITS	NOTES
	30	50	70		
Tensile Strength at Break	26	107	191	psi	ASTM D 412-06a
Elongation at Break	334	765	388	%	ASTM D 412-06a
Tensile Strength at 100% Strain	6	13	58	psi	ASTM D 412-06a
Tensile Strength at 200% Strain	12	24	113	psi	ASTM D 412-06a
Tensile Strength at 300% Strain	21	40	156	psi	ASTM D 412-06a
Compressive Stress at 10% Strain	0.9	2.7	11.8	psi	ASTM D 575-91, Method A
Compressive Stress at 20% Strain	2.1	6.4	30.0	psi	ASTM D 575-91, Method A
Compression Set	10	3	2	%	ASTM D 395
Tear Strength	12	28	27	lb/in	ASTM D 624-00, Die C
Bulk Modulus	4.5	5.0	4.3	gPascal	
Density	83	84	85	lb/ft ³	ASTME D 792-13
Specific Gravity	1.330	1.36	1.36		ASTME D 792-13
Optimum Performance Temperature Range	-20° to +140°	-20° to +150°	-20° to +160°	°F	Reduced strength and damping up to 200°F. Increased spring rate down to glass transition temperature.
Glass Transition	-20	-25	-17	°C	ASTM E 1640-13 by Peak Tan Delta
Flash Ignition Flammability	570°	570°	570°	°F	
Self Ignition Flammability	750°	750°	750°	°F	
Tested Flammability Rating with Retardant	V2	V2	V2		Underwriters Laboratory UL-94 (burns but self-extinguishing when flame removed)
Resilience Test Rebound Height	5	12	27	%	ASTM D 2632-92
Resilience Test Rebound Height	4	11	25	%	ASTM D 2632-92. Modified for the effects of material tackiness.
Dielectric Strength	213	250	252	V/ml	ASTM D 149-13, Method A
Dyanmic Young's Modulus at 5 Hertz	36, 41, 48	77, 89, 106	186, 209, 240	psi	Dyanmic Young's Modulus at 5 Hertz at 10%, 15%, 20%
Dyanmic Young's Modulus at 15 Hertz	57, 64, 75	113, 129, 154	186, 258, 295	psi	Dyanmic Young's Modulus at 15 Hertz at 10%, 15%, 20%
Dyanmic Young's Modulus at 30 Hertz	76, 86, 100	145, 165, 195	266, 299, 342	psi	Dyanmic Young's Modulus at 30 Hertz at 10%, 15%, 20%
Dyanmic Young's Modulus at 50 Hertz	95, 105, 119	175, 199, 231	298, 334, 382	psi	Dyanmic Young's Modulus at 50 Hertz at 10%, 15%, 20%
Tangent Delta at 5 Hz Excitation	0.72	0.57	0.28		
Tangent Delta at 15 Hz Excitation	0.78	0.62	0.33		
Tangent Delta at 30 Hz Excitation	0.80	0.64	0.36		
Tangent Delta at 50 Hz Excitation	0.80	0.65	0.37		
Bacterial Resistance	No Growth	No Growth	No Growth		ASTM G 21-09
Fungal Resistance	No Growth	No Growth	No Growth		ASTM G 22
Heat Aging	Stable	Stable	Stable		72 hours @ 158°F shows no change in size, appearance or durometer
Ultraviolet					Can be compounded for resistance
Acoustic Properties: Transmission Loss in Air	greater than 40	greater than 40	greater than 40	decibel/cm	At 50 Hz. Transmission loss increases with frequency

continued on next page



**Material Properties
of Sorbothane®**

EFFECTIVE 6/1/18

PROPERTY	DUROMETER (Shore 00)			UNITS	NOTES
	30	50	70		
Chemical Resistance to Distilled Water	51.6	42.1	23.8	% wt change	ASTM D 543, 7-day immersion
Chemical Resistance to City Water	50.7	41.8	23.7	% wt change	ASTM D 543, 7-day immersion
Chemical Resistance to Hydraulic Fluid	-4.8	-3.9	-4.2	% wt change	ASTM D 543, 7-day immersion
Chemical Resistance to Kerosene	-8.4	-4.9	-6.1	% wt change	ASTM D 543, 7-day immersion
Chemical Resistance to Diesel	-4.7	-1.4	23.7	% wt change	ASTM D 543, 7-day immersion
Chemical Resistance to 50% Ethanol	98.5	58.4	51.9	% wt change	ASTM D 543, 7-day immersion
Chemical Resistance to Soap Solution	100.4	59.4	33.0	% wt change	ASTM D 543, 7-day immersion
Chemical Resistance to Gasoline	37.9	40.6	41.7	% wt change	ASTM D 543, 7-day immersion
Chemical Resistance to Turpentine	14.5	16.3	13.4	% wt change	ASTM D 543, 7-day immersion
Chemical Resistance to Motor Oil 15W40	-4.4	-3.9	-4.1	% wt change	ASTM D 543, 7-day immersion
Chemical Resistance to Hexane	-5.1	-7.4	-2.8	% wt change	ASTM D 543, 7-day immersion
Chemical Resistance to IRM 903	-4.3	2.9	-3.7	% wt change	ASTM D 543, 7-day immersion
Chemical Resistance to 1N Acetic Acid	Complete Degradation	Complete Degradation	Complete Degradation	% wt change	ASTM D 543, 7-day immersion
Chemical Resistance to Ethylene Glycol	-1.1	0.2	0.4	% wt change	ASTM D 543, 7-day immersion
Chemical Resistance to 1N NaOH	11.9	10.7	7.2	% wt change	ASTM D 543, 7-day immersion

Appendix H

MATLAB Code

First, all constants was defined, figure H.1

```
E = 210e+9;
I = 3.0383e-05;
EI = E*I; %[Nm^2] Beam's stiffness
g = 9.81; %[m/s^2] gravitational acceleration
Q = 22500/2 * g;      %[N] Axle load one wheel
v = 70;             %[m/s] Velocity
k_padding = 50e+6/0.6;      %[120N/m] Spring padding
k_ballast = 65e+6;        %[N/m] Spring ballast
c_padding = 5e+3/0.6;      %[Ns/m] Damper padding
c_ballast = 150e+3;       %[Ns/m] Damper ballast
keq = (k_padding * k_ballast)/(k_ballast + k_padding);
ceq = (c_padding * c_ballast)/(c_ballast + c_padding);
Lt = v/2;              %[m] Length of transition zone
Lc = sqrt(sqrt(4*EI/keq)); %[m] Charachteristic length
A = 7.65093e-3;
mu = 7850;
rho = mu*A;%60.34;    %[kg/m] Mass per length
lambda = 1/Lc; % Static wave charachteristic
w0 = Q/(8*EI); % Max Static deflection
%v_cr = ((keq*EI)/(rho^2))^1/4; % Critical Velocity
v_cr = sqrt(2/rho * sqrt(keq * EI));
c_cr = 2*sqrt(keq*rho);% Critical damping
%a0 = v/(2*lambda)*sqrt(m/E*I); %[-] Speed ratio
%b0 = ceq/(2*m)*sqrt(m/keq); %[-] Damping ratio
a0 = v/v_cr; %Velocity ratio
b0 = ceq/c_cr; % Damping ratio
```

Figure H.1: Defining all constants needed to perform the computational analysis.

Translating the the fourth order equation from the analytical formulation into MATLAB programming language, figure H.2.

```

syms eta
n = solve(eta^6 + 2*alpha^2*eta^4 + (alpha^4 - 1)*eta^2 - alpha^2*beta^2,eta,'MaxDegree',6);
n = real(vpa(n));
n = abs(n);
n=max(n);
syms y
CharEq = y^4 + 4*(lambda*alpha).^2*y^2 -8*alpha*beta*lambda^3*y + 4*lambda^4; %Characteristic equation
Roots = solve(CharEq, y,'MaxDegree', 4); %Finding the roots
r = vpa(Roots); %Numerical values of roots
realRoots = real(r);
imaginaryRoots = imag(r);
a1 = n*lambda;
b2 = sqrt(lambda^2.*n^2 - (2*alpha * beta* lambda^2)/(n) + 2*alpha^2*lambda^2);
b1 = sqrt(lambda^2.*n^2 + (2*alpha * beta* lambda^2)/(n) + 2*alpha^2*lambda^2);
C2 = (Q*n)/(4*EI*lambda^2*(2*n^6-2*alpha^2*lambda*n^4+alpha^2*beta^2*lambda));
C1 = (n^3-alpha*beta)/(lambda*n*(n^3 + 2*alpha^2*n + 2*alpha*beta))*C2;
C3 = -(n^3 + alpha*beta)/(lambda*n*(n^3 + 2*alpha^2*n - 2*alpha*beta))*C2;
s = -10:0.05:10;
w1 = exp(-a1.*s).*(C1.*sin(b2.*s)+C2.*cos(b2.*s));
w2 = exp(a1.*s).*(C3.*sin(b1.*s)+C2.*cos(b1.*s));
w = length(w1);

for i = 1:length(s)
    if s(1,i)>=0
        w(i) = 1000*w1(i);
    else
        w(i) = 1000*w2(i);
    end
end
end

```

Figure H.2: Solving the equation computationally using MATLAB.

And finally producing the graphs figure H.3

```

figure(1)
plot(s,-w,'b-')
xlabel 'Rel. Distance from load';
ylabel 'Displacement [mm]';
legend = 'Displacement';
title('Deflection')
grid on
M = -diff(diff(w))/1000 * EI;
s = s(2:end-1);
figure(2)
plot(s,M,'-r')
title('Moment')
xlabel 'Rel. Distance from Load';
ylabel 'Moment [Nm]';
grid on;
ctrykk = 90.05/1000; %[m] Distance to the neutral axix
cstrekk = -80.95/1000;
sigmatrykk = M * ctrykk/I; %[Pa]
sigmatrykk = sigmatrykk/10^3; %[KPa]
sigmastrekk = M* cstrekk/I;
sigmastrekk = sigmastrekk/10^3;
figure(3)
hold on
plot(s,sigmatrykk, "-ma")
plot(s,sigmastrekk, "-g")
title('Bending Stress \sigma_b')
xlabel 'Rel. Distance from Load'
ylabel '\sigma_b [KPa]'
plot(0,max(sigmatrykk),'ob')
plot(0,min(sigmastrekk),'ob')
grid on
hold off

```

Figure H.3: Generating the graphs

Appendix I

Other Simulations

I.1 7 Meter Beam With 3 Point Distributed Load

The same 7 meter long beam with identical connections, fixtures and time step was in addition subjected to a 3 point distributed load.

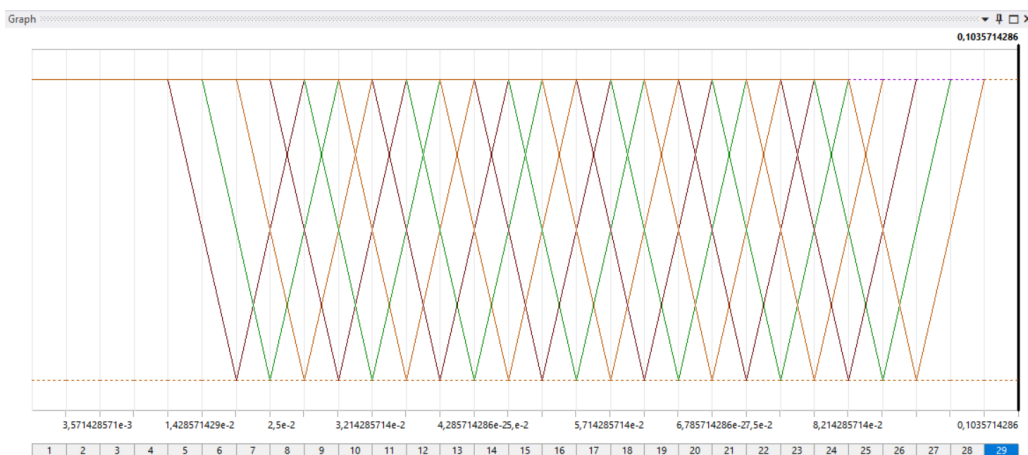


Figure I.1: The force over time graph.

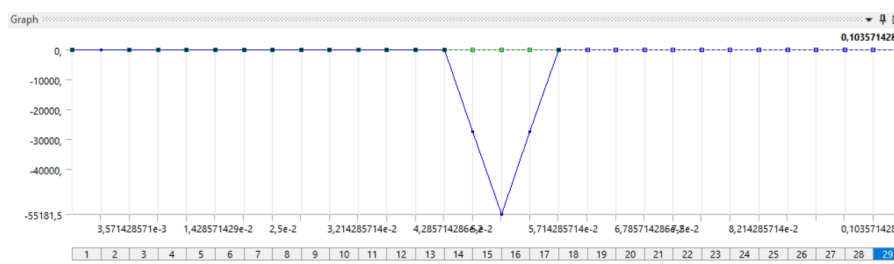


Figure I.2: Force distributed over 3 nodes graph.

The maximum deformation after the 3 point distributed load were applied was 0.60 mm. This result is not surprising as the locally point force of -110363 N is distributed.

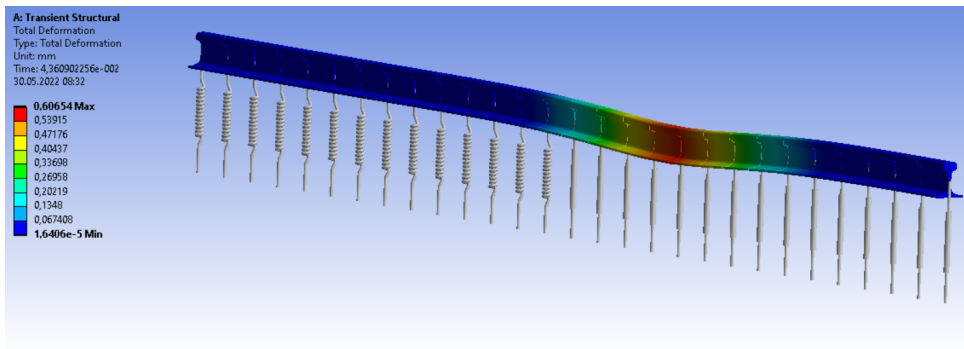


Figure I.3: The maximum deformation of the distributed load

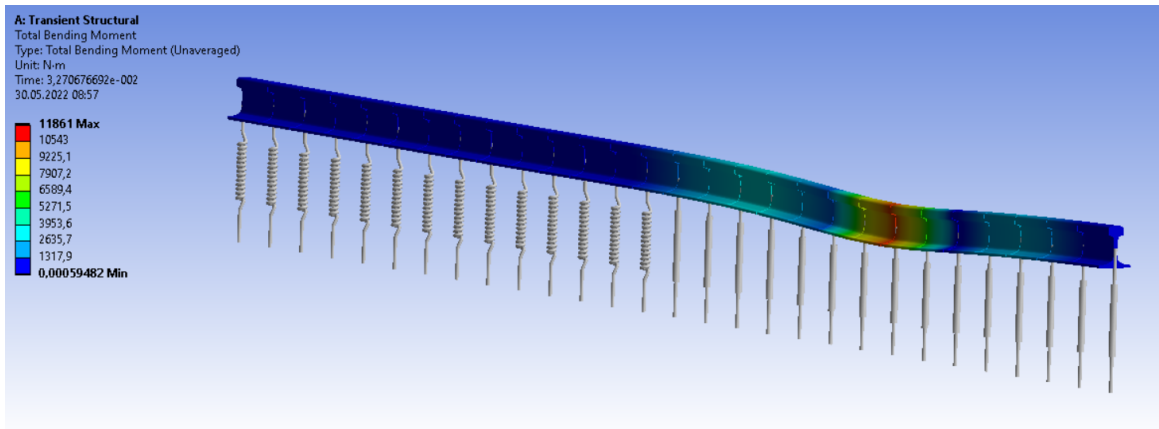


Figure I.4: Maximum bending moment

The maximum bending moment 11.86 kNm for the 3 point distributed load.

I.2 1 Meter Beam With Point Load

A beam with a length of 1000 mm were tested to see the curvature in the beam. The element size was set to 15 mm. This beam with a point load, 3 point load and a 9 point load. The total nodes for this beam were counted to be 68. The time step for this beam was calculated to be $\approx 2.1 \times 10^{-4}$ seconds. The train will ride over this beam in about 0.0143 seconds since the velocity is 70 m/s.

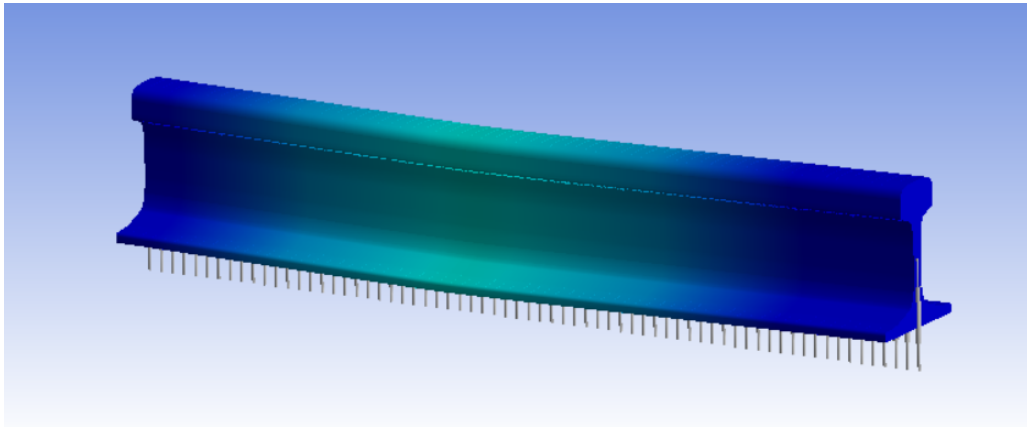


Figure I.5: Deformation of the beam

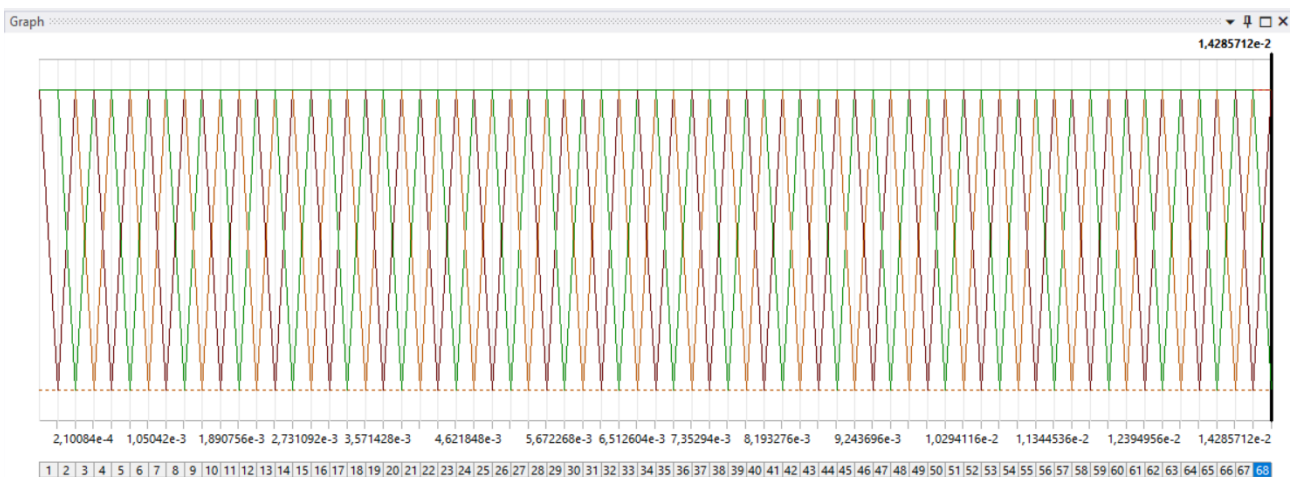


Figure I.6: Force distribution over time

I.3 1 Meter Beam with 3 Point Distributed Load

The load in this beam was distributed over three nodes at each time step. As figure I.7 shows, there are no significant deformation.

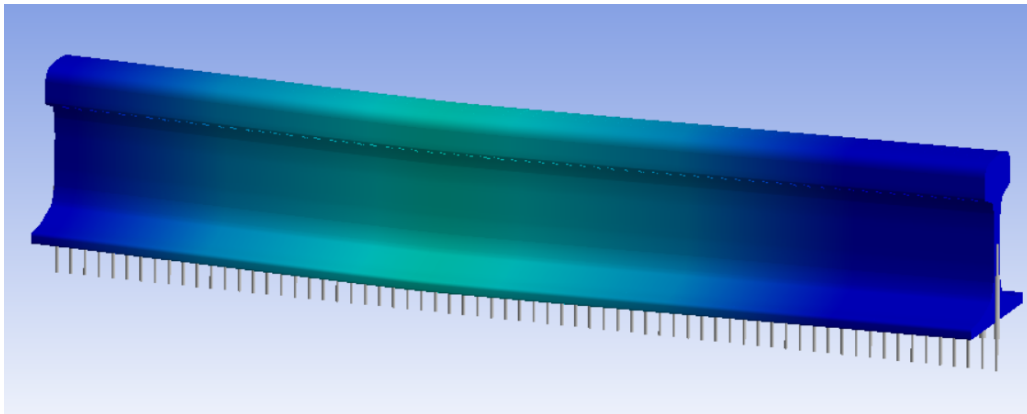


Figure I.7: Deformation of the beam when 3 point load was applied

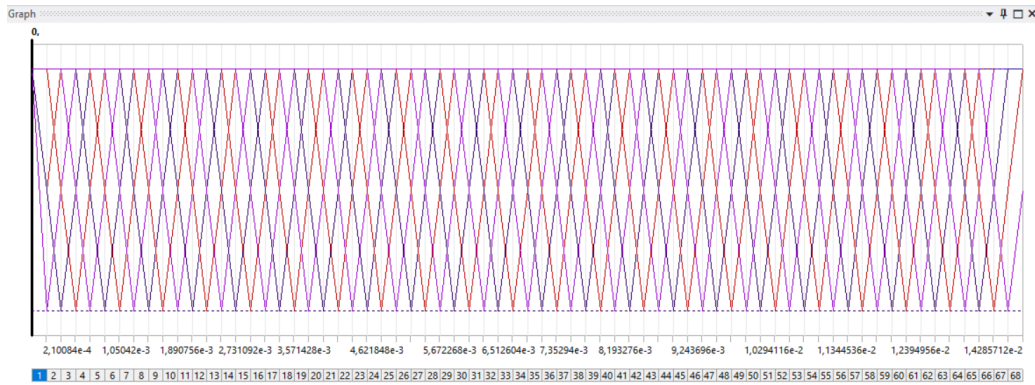


Figure I.8: Force distribution over time when 3 point loads were applied

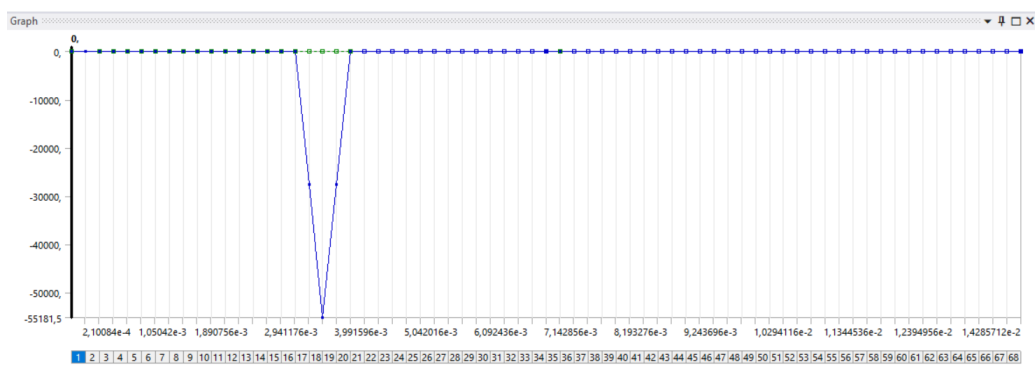


Figure I.9: The graph depicts how the 3 point load at a time step looks like

1 Meter Beam With 9 Point Distributed Load

In the 9 point load case the force graph took another form, see figure I.10

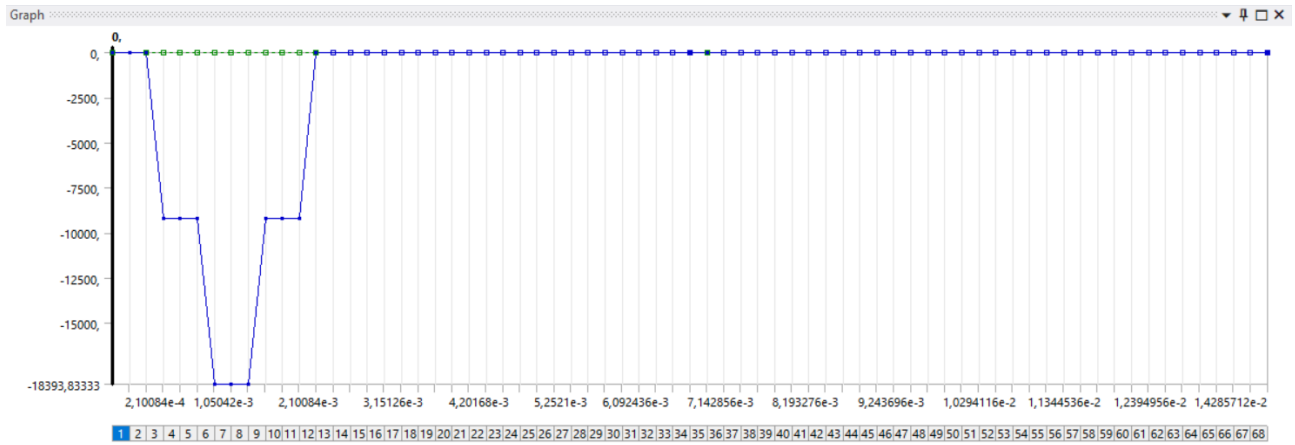


Figure I.10: The figure illustrates how the distributed 9 load load were applied at a time step.

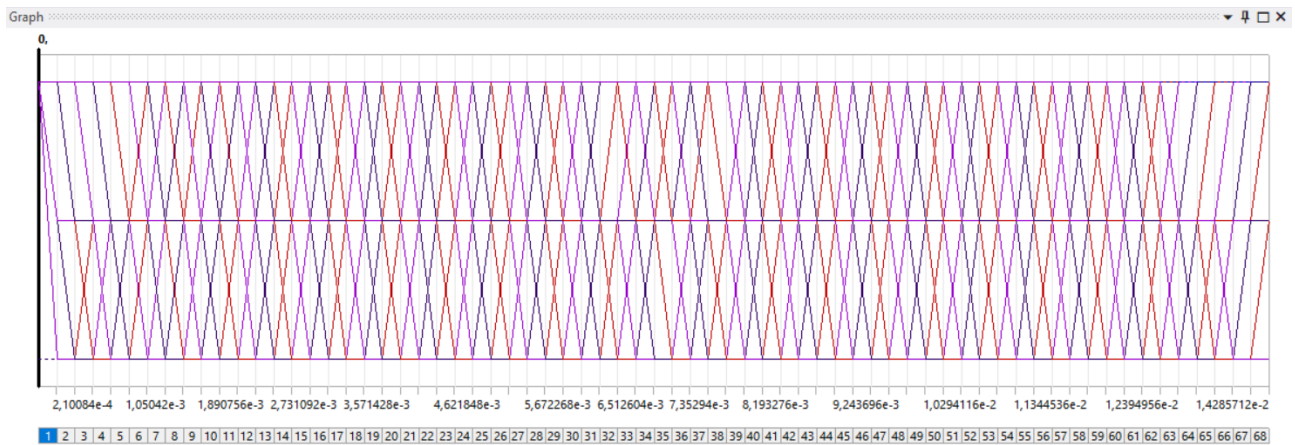


Figure I.11: The graph is showing how the distributed load looked like vs. time.

I.4 35 Meter Beam With Point Load

The whole transition zone was also analyzed. The total element size of 500 mm which resulted in 70 elements. Same spring and damper were applied as for the other cases. The train will transverse the whole transition zone in 0.5 seconds which means that the time steps for this beam was $\approx 7.14 \times 10^{-3}$ seconds.

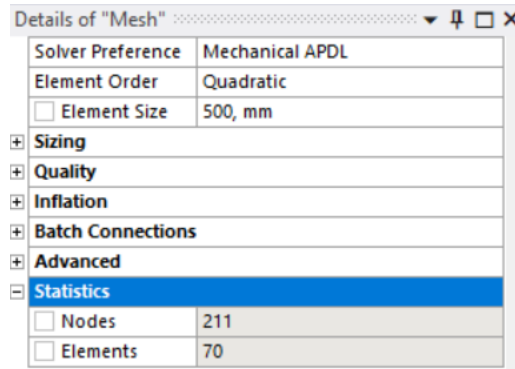


Figure I.12: Mesh details showing element size to be 500 mm and elements to be 70.

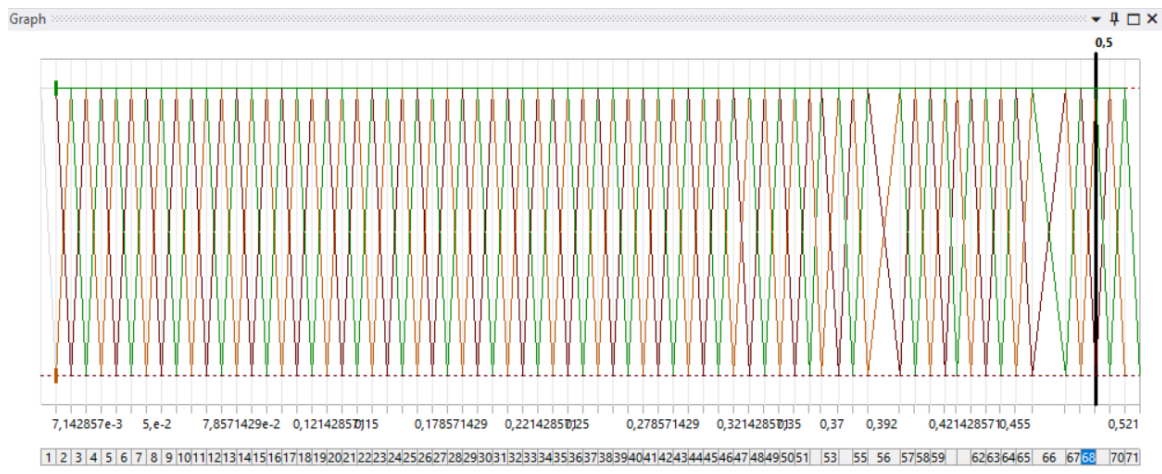


Figure I.13: Total force vs. time for 35 meter long beam.

Results	
<input type="checkbox"/> Minimum	0, mm
P <input checked="" type="checkbox"/> Maximum	1,028768778 mm
<input type="checkbox"/> Average	5,425040546e-002 mm
Minimum Occurs On	SYS\Beam (Extracted Profile1)
Maximum Occurs On	SYS\Beam (Extracted Profile1)
Minimum Value Over Time	

Figure I.14: Maximum deformation is showing to be

The maximum deflection for the 35 meter long beam does have a deformation that is somewhat close to the analytical with a deflection of 1.02 mm. However, it was decided that the element size of 500 mm would be too coarse to get an accurate reading. If the element size were halved, the element count would double to 140, which was decided not necessary.

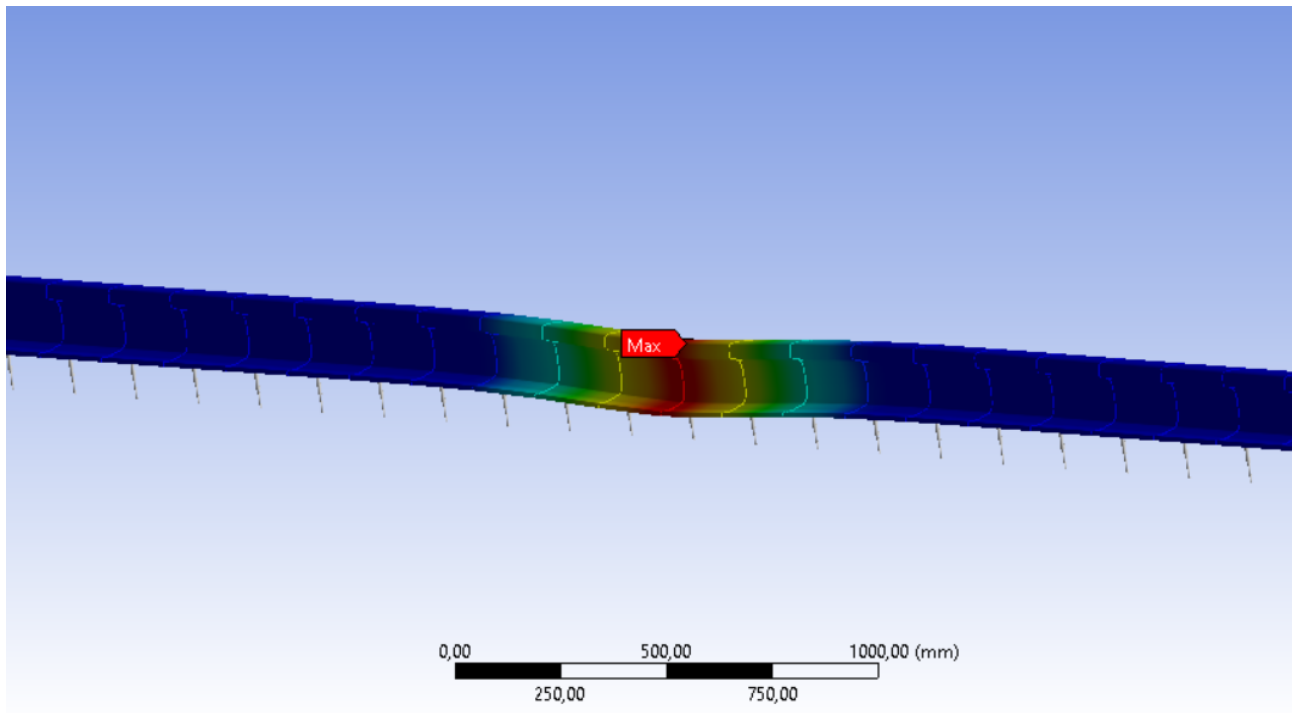


Figure I.15: Total deformation for the beam

